

**NIST Technical Note 2125**

**Pool Boiling of R514A, R1224yd(Z),  
and R1336mzz(E) on a Reentrant  
Cavity Surface; Extensive  
Measurement and Analysis**

Mark A. Kedzierski  
Lingnan Lin

This publication is available free of charge from:  
<https://doi.org/10.6028/NIST.TN.2125>

**NIST**  
**National Institute of  
Standards and Technology**  
U.S. Department of Commerce

NIST Technical Note 2125

**Pool Boiling of R514A, R1224yd(Z),  
and R1336mzz(E) on a Reentrant  
Cavity Surface; Extensive  
Measurement and Analysis**

Mark A. Kedzierski  
Lingnan Lin  
*Energy and Environment Division  
Engineering Laboratory*

This publication is available free of charge from:  
<https://doi.org/10.6028/NIST.TN.2125>

December 2020



U.S. Department of Commerce  
*Wilbur L. Ross, Jr., Secretary*

National Institute of Standards and Technology  
*Walter Copan, NIST Director and Undersecretary of Commerce for Standards and Technology*

Certain commercial entities, equipment, or materials may be identified in this document in order to describe an experimental procedure or concept adequately. Such identification is not intended to imply recommendation or endorsement by the National Institute of Standards and Technology, nor is it intended to imply that the entities, materials, or equipment are necessarily the best available for the purpose.

**National Institute of Standards and Technology Technical Note 2125**  
**Natl. Inst. Stand. Technol. Tech. Note 2125, 41 pages (December 2020)**  
**CODEN: NTNOEF**

**This publication is available free of charge from:**  
**<https://doi.org/10.6028/NIST.TN.2125>**

# Pool Boiling of R514A, R1224yd(Z), and R1336mzz(E) on a Reentrant Cavity Surface; Extensive Measurement and Analysis

M. A. Kedzierski, and L. Lin  
National Institute of Standards and Technology  
Gaithersburg, MD 20899

## ABSTRACT

This paper quantifies the pool boiling performance of R514A, R1224yd(Z), and R1336mzz(E) on a flattened, horizontal Turbo-ESP surface for air-conditioning applications for heat fluxes between roughly  $10 \text{ kWm}^{-2}$  and  $100 \text{ kWm}^{-2}$ . R514A, R1224yd(Z), and R1336mzz(E) are replacements for R123 and R245fa. All of these replacement refrigerants had measured boiling heat fluxes that were larger than that for R123 for most heat fluxes. For example, for heat fluxes between  $10 \text{ kWm}^{-2}$  and  $80 \text{ kWm}^{-2}$ , R514A, R1224yd(Z), and R1336mzz(E) exhibited average heat fluxes that were 30 %, 57 %, and 13 % larger than that for R123 for a saturation temperature of 277.6 K. For the same comparison done at a saturation temperature of 298.2 K, the average heat flux for R514A was roughly 43 % larger than that for R123. A pool boiling model, that was previously developed for pure and mixed refrigerants on the Turbo-ESP surface, was compared to the measured boiling performance. The model predicted the measured superheats of the mixed refrigerants and the single component refrigerants to within  $\pm 0.7 \text{ K}$  and  $\pm 0.45 \text{ K}$ , respectively.

Keywords: boiling, enhanced heat transfer, refrigerants, structured surface

## TABLE OF CONTENTS

<b>ABSTRACT</b> .....	iii
<b>TABLE OF CONTENTS</b> .....	iv
<b>LIST of figures</b> .....	iv
<b>List of tables</b> .....	v
<b>INTRODUCTION</b> .....	1
<b>APPARATUS</b> .....	3
<b>TEST SURFACE</b> .....	3
<b>MEASUREMENTS AND UNCERTAINTIES</b> .....	4
<b>EXPERIMENTAL RESULTS</b> .....	5
<b>COMPARISON TO POOL BOILING MODEL</b> .....	7
<b>CONCLUSIONS</b> .....	10
<b>ACKNOWLEDGEMENTS</b> .....	11
<b>NOMENCLATURE</b> .....	12
<b>English Symbols</b> .....	12
<b>Greek symbols</b> .....	12
<b>English Subscripts</b> .....	12
<b>REFERENCES</b> .....	13

## LIST OF FIGURES

<b>Fig. 1 Schematic of test apparatus</b> .....	24
<b>Fig. 2 OFHC copper flat test plate with Turbo-ESP surface and thermocouple coordinate system</b> .....	25
<b>Fig. 3 Photograph of Turbo-ESP surface</b> .....	26
<b>Fig. 4 Comparison of boiling curves for R514A, and R1336mzz(Z) at 277.6 K and 298.2 K</b> .....	27
<b>Fig. 5 Comparison of R514A heat fluxes for different saturation temperatures to that for R123 at the same wall superheat</b> .....	28
<b>Fig. 6 Comparison of boiling curves for R1336mzz(E) and R1224yd(Z) at 277.6 K</b> .....	29
<b>Fig. 7 Comparison of R1224yd(Z) and R1336mzz(E) heat fluxes to that for R123 at the same wall superheat</b> .....	30
<b>Fig. 8 Comparison of pool boiling model for Turbo-ESP surface to present measurements for R1224yd(Z) and R1336mzz(E)</b> .....	31
<b>Fig. 9 Comparison of refrigerant mixture pool boiling model for Turbo-ESP surface to R514A measurements</b> .....	32
<b>Fig. 10 Illustration of effect of key properties on pool boiling model heat flux</b> .....	33
<b>Fig. A.1 Expanded relative uncertainty in the heat flux of the surface at the 95 % confidence level</b> .....	34
<b>Fig. A.2 Expanded uncertainty in the temperature of the surface at the 95 % confidence level</b> .....	35

## LIST OF TABLES

<b>Table 1</b>	<b>Conduction model choice.....</b>	<b>16</b>
<b>Table 2</b>	<b>Pool boiling data.....</b>	<b>17</b>
<b>Table 3</b>	<b>Number of test days and data points.....</b>	<b>22</b>
<b>Table 4</b>	<b>Estimated parameters for cubic boiling curve fits.....</b>	<b>22</b>
<b>Table 5</b>	<b>Residual standard deviation of <math>\Delta T_s</math>.....</b>	<b>22</b>
<b>Table 6</b>	<b>Average magnitude of 95 % multi-use confidence interval for mean <math>\Delta T_s</math>.....</b>	<b>23</b>
<b>Table 7</b>	<b>Selected fluid properties of test refrigerants at saturation (277.6 K) using REFPROP 10.0 default equations (Lemmon et al., 2018).....</b>	<b>23</b>

## INTRODUCTION

Currently, the air-conditioning and refrigeration industry is in pursuit of fourth-generation refrigerants in order to comply with low global warming potential (GWP) mandates set by the European F-gas Regulation (EU, 2014) and the Kigali amendment to the Montreal Protocol (UNEP, 2016). The search has been difficult because new refrigerants must have numerous qualities to ensure the efficient and reliable operation of cooling equipment. For example, a refrigerant must meet the required temperature, pressure, enthalpy, and heat transfer characteristics while remaining stable and environmentally benign. The Montreal Protocol (1987) set regulations that limited the ozone depletion potential (ODP) of refrigerants, which lead to zero ODP, third-generation refrigerants like R123 and R245fa. The new regulations (EU (2014) and UNEP, 2016) have caused a recent shift to refrigerants with both zero ODP and low GWP. Refrigerants R123 (ODP = 0.01, GWP<sup>1</sup> = 80 (WMO, 2018)) and R245fa (ODP = 0, GWP = 880 (WMO, 2018)) are low-pressure refrigerants that have been used chiefly in water chillers that cool large buildings. In addition, R245fa has been used as a working fluid in organic Rankine cycles (Kontomaris, 2014). Yang et al. (2019) have demonstrated the viability of R1336mzz(E) in Rankine cycles as a replacement for R245fa. The new refrigerant R1336mzz(E) has the advantage over R123 and R245fa of having a zero ODP and a GWP of 16 (WMO, 2018). Kontomaris (2019) proposed the use of R514A in a Rankine cycle, which is a near-azeotropic mixture, of 74.7 % R1336mzz(Z) and 25.3 % R1130, on a mass basis. Both R514A and R1224yd(Z) are proposed replacements for R123 and R245fa with zero ODP. The GWP for R514A is 2 (Myhre et al., 2013) and that for R1224yd(Z) is 0.88 (Tokuhashi et al., 2018).

To facilitate the use of new low GWP refrigerants in water chillers and Rankine cycles, this paper investigates the boiling heat transfer performance of R514A, R1224yd(Z), and R1336mzz(E) on the Turbo-ESP<sup>2</sup>. Boiling measurements on the Turbo-ESP ensures the relevance of this investigation for commercial chillers because it is one of the newer boiling surfaces. The Turbo-ESP surface is a highly modified version of a rectangular-finned surface. Rectangularly finned tubes, with low fin densities, were the very first commercial application of refrigerant-shell-side enhancements to water chillers, which occurred around 1938 (Rogers, 1961). Significant improvement of the heat transfer performance occurred in 1971 with the introduction of the “bent fin,” which was a commercial boiling tube that was made specifically for the promotion of reentrant boiling (Kedzierski, 1999). The bent fin tube was created with a simple modification of the rectangularly finned tube by raking the fins back upon themselves producing a specified gap between the fin-tip and the adjacent fin for escaping bubbles, as further explained in US patent 3,696,861 (Webb, 1972). Continued evolution of enhanced boiling tube technology has led to significantly more intricate surfaces than the bent fin, with more complicated fin shapes and larger fin densities like the Turbo-ESP.

Only a few studies can be found in the literature that provide pool boiling measurements on the Turbo-ESP surface. Gorgy (2016) gives measurements for R123, R134a, R1234ze(E), R1233zd(E), and R450A on the Turbo-ESP surface. Gorgy (2016) found that the performance of R1234ze(E) is very similar to that of R134a while R450A exhibits a performance degradation

---

<sup>1</sup> All GWP values are given for zero contribution from climate-carbon feedbacks and 100-year horizons.

of 28% as compared to R134a. Gorgy (2016) also showed that the boiling heat transfer for R1233zd(E) was 19% greater than that for R123. Kedzierski and Lin (2020a) provided pool boiling measurements for R515A, R1234ze(E), and R1233zd(E) on the Turbo-ESP surface. The measured boiling curve for R515A had roughly a 14 % larger heat flux than that of R1234ze(E) for heat fluxes greater than 45 kWm<sup>-2</sup>. For heat fluxes between 14 kWm<sup>-2</sup> and 85 kWm<sup>-2</sup>, R515A and R1234ze(E) exhibited a heat flux that was 33 % and 17 % larger than that for R134a. The heat flux of R1233zd(E) was roughly 18 % larger than that for R123 between 30 kWm<sup>-2</sup> and 87 kWm<sup>-2</sup>. Kedzierski and Lin (2020a) updated their pool boiling model for pure and mixed refrigerants for the Turbo-ESP surface and showed that the vapor Prandtl number and the product of the latent heat and vapor density significantly influenced the boiling heat flux. More boiling measurements were made on the Turbo-ESP surface by Kedzierski and Lin (2020b) in a study of the influence of inorganic fullerene-like tungsten disulfide (IF-WS<sub>2</sub>) nanoparticles on the pool-boiling performance of R134a/polyolester mixtures. The study showed that the nanolubricant caused an average 37 % degradation in the boiling heat flux as compared to R134a/neat-lubricant boiling on the Turbo-ESP surface at the same superheat. They presented an analysis that showed that the nanoparticles were too large and too dense to promote a boiling enhancement. In other work, Kedzierski and Lin (2019) quantified the pool boiling performance of R1336mzz(Z) on the Turbo-ESP surface and showed that the boiling performance of R1336mzz(Z) did not differ statistically from that of R123 for heat fluxes between 13 kWm<sup>-2</sup> and 59 kWm<sup>-2</sup>. For heat fluxes larger than 59 kWm<sup>-2</sup>, the R123 boiling heat flux was up to 5 % larger than the heat flux for R1336mzz(Z). They developed a pool boiling model to predict boiling heat transfer for the test refrigerants on the Turbo-ESP surface, mostly, to within ± 0.5 K. Finally, Kedzierski et al. (2018) measured the pool boiling performance of R134a, R1234yf, R513A, and R450A for the Turbo-ESP. On average, the heat flux for R1234yf and R513A was 16 % and 19 % less than that for R134a, respectively, for R134a heat fluxes between 20 kWm<sup>-2</sup> and 110 kWm<sup>-2</sup>. The heat flux for R450A was on average 57 % less than that of R134a for heat fluxes between 30 kWm<sup>-2</sup> and 110 kWm<sup>-2</sup>.

Because of the relatively recent introduction of R514A, R1224yd(Z), and R1336mzz(E), no pool boiling studies were found for any of these refrigerants. Only one study (Longo et al., 2019) was found that investigated the heat transfer of R1224yd(Z). Longo et al. (2019) measured the flow boiling heat transfer and pressure characteristics of R1224(Z) within a micro-fin tube with internal fin-tip diameter of 4.2 mm. They found that the forced convection mechanism prevailed over the nucleate boiling mechanism for most conditions. No heat transfer studies were found in the literature that were associated with either R514A or R1336mzz(E). The studies on R1336mzz(E) in the literature mostly focused on the thermodynamics properties measurement. For example, Tanaka et al. (2017a) measured and correlated the critical parameters and vapor pressure of R1336mzz(E). In another study, Tanaka et al. (2017b) measured the pressure, density, and temperature of R1336mzz(E) by the isochoric method. Only a single study on the chemical stability of R514A was found in the literature (Majurin et al., 2017). They found that R514A perform similar to or better than

---

<sup>2</sup> Certain trade names and company products are mentioned in the text or identified in an illustration in order to adequately specify the experimental procedure and equipment used. In no case does such an identification imply recommendation or endorsement by the National Institute of Standards and Technology, nor does it imply that the products are necessarily the best available for the purpose.

R123 in accelerated reaction tests, a contaminant study, and a chiller refrigerant and lubricant evaluation. Considering the very limited data, the present study provides pool boiling heat transfer measurements for R514A, R1224yd(Z), and R1336mzz(E) on the horizontal, flat, copper, Turbo-ESP-finned surface for test conditions that are applicable for air-conditioning applications.

## APPARATUS

Figure 1 shows a schematic of the apparatus that was used to collect the pool boiling data. More specifically, the apparatus was used to measure the liquid saturation temperature ( $T_s$ ), the average pool-boiling heat flux ( $q''$ ), and the wall temperature ( $T_w$ ) of the test surface. The three principal components of the apparatus were a test chamber containing the test surface, the condenser, and the purger. The internal dimensions of the aluminum test chamber were approximately 25 mm  $\times$  257 mm  $\times$  1540 mm. As shown in Fig. 1, the test section was visible through two opposing, flat 150 mm  $\times$  200 mm quartz windows. The test chamber was charged with approximately 7 kg of refrigerant, giving a liquid height of approximately 80 mm above the test surface as viewed through the windows. The specified liquid height fixed the local vapor quality and the hydrostatic pressure above the surface for a given heat flux for between-run tests and for tests between fluids. The bottom of the test surface was heated with high velocity (roughly 2.5 m/s) water flow. The vapor produced by liquid boiling on the test surface was condensed by the brine-cooled, shell-and-tube condenser and returned as liquid to the pool by gravity. Further details of the test apparatus can be found in Kedzierski (2002) and Kedzierski (2001).

One of the important aspects of the present boiling measurements is that they were produced by fluid heating to provide measurements with the same heating boundary condition as experienced by real-world heat exchange equipment. The studies of Kaul et al. (1996) and Darabi et al. (1999) warn that electrically heated flow boiling measurements should be used with caution because the results can potentially differ from those obtained from fluid heating. Likewise, Kedzierski (1995) has shown that the fluid and the electrically heated boundary conditions can produce pool boiling heat fluxes that differ by as much as 32 % for the same superheat with all other conditions fixed. Thus, to provide designers data with a heating boundary condition that is applicable to their heat exchangers, only fluid heating was used to elevate the temperature of the test surface to produce boiling in this study.

## TEST SURFACE

Figure 2 shows the oxygen-free high-conductivity (OFHC) copper flat test plate used in this study. The test plate was machined out of a single piece of OFHC copper by electric discharge machining (EDM). The internal fins of a commercial 25 mm (outer-diameter) Turbo-ESP tube were removed by EDM to produce a tube with a smooth inner wall and a reentrant cavity surface on the outer wall. The tube was then cut axially, annealed, flattened, and soldered onto the top of the test plate. The Turbo-ESP has approximately 1968 fins per meter (fpm) oriented along the short axis of the plate with an approximate fin-thickness of 0.2 mm. Figure 3 shows a photograph of the fin surface and identifies three key geometry parameters: the fin, the gap between fins at the fin-tips, and the slot openings at the fins. The overall fin-height, the gap at the fin-tips, and the width of the fin slots are approximately 0.4 mm, 0.04 mm, and 0.05 mm, respectively. The fin-gap and the fin-slots establish the

opening size for the exiting bubbles, which are typically sized depending on the surface tension of the boiling fluid. For this reason, the fin-gap and the width of the fin-slot are approximately the same.

## MEASUREMENTS AND UNCERTAINTIES

The standard uncertainty is the square root of the estimated variance. The individual standard uncertainties are combined to obtain the expanded uncertainty ( $U$ ), which is calculated from the law of propagation of uncertainty with a coverage factor. All measurement uncertainties are reported at the 95 % confidence level except where specified otherwise. Further detail on the heat transfer measurement uncertainties can be found in Appendix A.

All of the copper-constantan thermocouples and the data acquisition system were calibrated against a glass-rod standard platinum resistance thermometer (SPRT) and a reference voltage to a residual standard deviation of 0.005 K. The reference voltage enabled the correction of any drift in the voltage measurement over time. Considering the fluctuations in the saturation temperature during the test and the standard uncertainties in the calibration, the expanded uncertainty of the average saturation temperature was no greater than 0.04 K. Consequently, it is estimated that the expanded uncertainty of the temperature measurements was less than 0.1 K.

Twenty 0.5 mm diameter thermocouples were force fitted into the wells of the side of the test plate shown in Fig. 2. The heat flux and the wall temperature were obtained by regressing the measured temperature distribution of the block to the governing two-dimensional conduction equation (Laplace equation). In other words, rather than using the boundary conditions to solve for the interior temperatures, the interior temperatures were used to solve for the boundary conditions following a backward stepwise procedure given in Kedzierski (1995)<sup>3</sup>. As shown in Fig. 2, the origin of the coordinate system was centered on the surface with respect to the y-direction at the heat transfer surface. Centering the origin in the y-direction reduced the uncertainty of the wall heat flux and temperature calculations by reducing the number of fitted constants involved in these calculations.

Fourier's law and the fitted constants from the Laplace equation were used to calculate the average heat flux ( $q''$ ) normal to and evaluated at the heat transfer surface based on its projected area. The average wall temperature ( $T_w$ ) was calculated by integrating the local wall temperature ( $T$ ). The wall temperature was approximately uniform having less than 0.1 K uncertainty for all but 33 out of 805 measurements. The wall superheat was calculated from  $T_w$  and the measured temperature of the saturated liquid ( $T_s$ ). Considering this, the relative expanded uncertainty in the heat flux ( $U_{q''}$ ) was greatest at the lowest heat fluxes, approaching 9 % of the measurement near 15 kWm<sup>-2</sup>. In general, the  $U_{q''}$  remained between 3 % and 6 % for heat fluxes greater than 20 kWm<sup>-2</sup>. The average random error in the wall superheat ( $U_{T_w}$ ) remained mainly between 0.02 K and 0.1 K with an average value of approximately 0.06 K. The measured thickness of the solder layer, which was used to attach

---

<sup>3</sup> Table 1 provides functional forms of the Laplace equation that were used in this study in the same way as was done in Kedzierski (1995) and in similar studies by this author.

the flattened tube to the copper plate, was less than 0.1 mm and was accounted for when calculating the measurements and the uncertainties following procedures as outlined in Kedzierski (1995). Plots of  $U_{q''}$  and  $U_{T_w}$  versus heat flux can be found in Appendix A.

## EXPERIMENTAL RESULTS

The pool-boiling measurements were made at two saturation temperatures: 298.2 K and 277.6 K. The rate of chilled brine flow to the condenser was adjusted to control the saturation temperature of the test fluid. The heat flux was varied between  $10 \text{ kWm}^{-2}$  and  $100 \text{ kWm}^{-2}$  to simulate a range of possible operating conditions for R123 and R245fa chillers. The data were recorded consecutively starting at the largest heat flux and descending in intervals of approximately  $4 \text{ kWm}^{-2}$ . The descending heat flux procedure minimized the possibility of observing any hysteresis effects on the data, which would have made the data sensitive to the initial operating conditions. Check out tests with R134a were done prior to each new study to ensure that the present boiling performance closely repeated previous measurements with R134a. Table 2 presents the measured heat flux and wall superheat for all the data of this study. Table 3 gives the number of test days and data points for each fluid. A total of 805 measurements were made over 33 days.

Figure 4 is a plot of the measured boiling heat flux ( $q''$ ) versus the measured wall superheat ( $T_w - T_s = \Delta T_s$ ) for R514A on the Turbo-ESP for two saturation temperatures: 277.6 K and 298.2 K. The open circles and open squares represent the measured data for R514A at 298.2 K and 277.6 K, respectively. The solid line is a cubic best-fit regression or estimated mean of the data. Twenty test days with R514A produced 498 measurements over a period of approximately two months. Twenty-one of the 498 measurements were removed before fitting because they were statistically identified as “outliers” based on having both high influence and high leverage (Belsley et al., 1980). The data sets for each test fluid presented in this manuscript exhibited a similar number of outliers and were regressed in the same manner. Surface aging data (i.e., “break-in” data) also were not included in the analyzed data sets. The surface aging data typically occurred for each fluid over the first or first and second test days and deviated significantly from the mean of the succeeding and consecutive measurements made over six to seven days. Surface aging measurements were believed to have been removed from analyzed data because the resulting between-run variation was mainly random.

Table 4 gives the constants for the cubic regression of the superheat versus the heat flux for all of the fluids tested here and the superheat range for which each regression is valid. The residual standard deviation of the regressions – representing the proximity of the data to the mean – are given in Table 5, and fall between 0.05 K and 0.11 K. The dashed lines to either side of the mean boiling curve (solid line), in Figs. 4 and 6, represent the lower and upper 95 % simultaneous (multiple-use) confidence intervals for the mean and are, for much of the data, concealed by the data symbols. Using the confidence intervals and the previously discussed temperature calibration, the expanded uncertainty of the estimated mean wall superheat was, on average,  $\pm 0.04 \text{ K}$ . Table 6 provides the average magnitude of the 95 % multi-use confidence interval for the fitted wall superheat for all of the test data, which varied between  $\pm 0.03 \text{ K}$  and  $\pm 0.05 \text{ K}$ .

Considering that R514A is 74.7/25.3 by mass mixture of R1336mzz(Z) and R1130, Fig. 4 compares the present pool-boiling measurements for R514A to the means of the R1336mzz(Z) pool boiling measurements from Kedzierski and Lin (2019) on the Turbo-ESP for the saturation temperatures of 277.6 K and 298.2 K. At the saturation temperature of 277.6 K, the boiling heat flux for R514A is nearly double that for R1336mzz(Z) at 1 K. The difference between the R514A and the R1336mzz(Z) heat fluxes decrease with respect to increasing superheat and is zero where the means intersect at a superheat of approximately 2.2 K. At a superheat of 2.7 K, the boiling heat flux of R1336mzz(Z) is approximately 5 % larger than that of R514A. At the saturation temperature of 298.2 K, the boiling heat flux for R514A is nearly double that for R1336mzz(Z) at 0.6 K. Similar to the 277.6 K saturation case, the difference between the R514A and the R1336mzz(Z) heat flux, for the 298.2 K condition, decreases with respect to increasing superheat and is zero where the means intersect at a superheat of approximately 0.9 K. At a superheat of 2.5 K, the boiling heat flux of R1336mzz(Z) is approximately 10 % larger than that of R514A.

Being that R514A is a replacement for R123, Fig. 4 provides the mean boiling curve for R123 at a saturation temperature of 277.6 K, as taken from Kedzierski and Lin (2018) and shown as a long-dashed black line. For a wall superheat of 0.9 K, the boiling heat flux of R514A is approximately twice that of R123. As the superheat increases, the heat flux difference decreases until it equals zero at a superheat of approximately 2 K. At a superheat of 2.6 K, the R123 heat flux is approximately 9 % larger than that for R514A at 277.6 K.

Figure 5 shows a more precise quantification of the boiling heat transfer rate of R514A for the two saturation temperatures relative to R123. Comparisons are made only to R123 at 277.6 K due to the lack of measurements for R123 at 298.2 K. Figure 5 plots the ratio of the R514A heat flux to the R123 heat flux from Kedzierski and Lin (2018) at the same wall superheat. The heat flux ratio is shown as a solid line with dashed lines representing the 95 % multi-use confidence level for each mean. A statistical difference in the heat transfer performance is confirmed where the 95 % simultaneous confidence intervals (depicted by the dashed lines) do not include the value one. The maximum heat flux ratios for R514A coincide with the lowest evaluated R123 heat flux of approximately  $10 \text{ kWm}^{-2}$ . By comparison, at  $10 \text{ kWm}^{-2}$ , the heat flux ratios are  $2.76 \pm 0.04$  and  $2.44 \pm 0.04$  for the 298.2 K and the 277.6 K saturation temperatures, respectively. At  $100 \text{ kWm}^{-2}$ , the heat flux ratios are  $1.05 \pm 0.02$  and  $0.92 \pm 0.02$  for the 298.2 K and the 277.6 K saturation temperatures, respectively. The relative difference between the heat flux ratios, for the two saturation temperatures, decreases from 32 % at  $10 \text{ kWm}^{-2}$  to roughly 13 % at  $20 \text{ kWm}^{-2}$ , and then remains relatively constant at 13 % between  $20 \text{ kWm}^{-2}$  and  $100 \text{ kWm}^{-2}$ . The average heat flux ratio for R514A between  $10 \text{ kWm}^{-2}$  and  $80 \text{ kWm}^{-2}$  was approximately 1.43 and 1.30 for saturation temperatures of 298.2 K and 277.6 K, respectively. The average heat flux ratio for R514A between  $10 \text{ kWm}^{-2}$  and  $30 \text{ kWm}^{-2}$  was approximately 1.93 and 1.78 for saturation temperatures of 298.2 K and 277.6 K, respectively.

Figure 5 illustrates that the boiling enhancement mechanism of the Turbo-ESP surface is most effective at low superheats for R514A as compared to R123. The relatively closed canopy of the Turbo-ESP surface encourages bubble coalescence and aids in the retention of relatively large vapor seeds within the reentrant cavities resulting in relatively low superheat

requirements for bubble generation (Kedzierski, 1995). As the superheat increases, the benefit of the passive enhancement benefit for the Turbo-ESP begins to become redundant because large superheats are associated with vigorous bubble interaction due to large bubble site-density. Consequently, any advantage a fluid boiling on the Turbo-ESP might have over another fluid in performance at low superheat is likely to be diminished, due to all fluids exhibiting a high level of bubble interaction, at high superheats.

Figure 6 compares the pool-boiling heat flux ( $q''$ ) for the Turbo-ESP surface versus the wall superheat ( $T_w - T_s$ ) measured in this study for R1336mzz(E) and for R1224yd(Z). Comparison of the mean boiling curves shows that the heat flux of R1224yd(Z) exceeds that of R1336mzz(E) by approximately  $17 \text{ kWm}^{-2}$ , on average. Figure 6 shows a similar average difference between R1224yd(Z) and the boiling curve for R123 as taken from Kedzierski and Lin (2018) and shown as a long-dashed line. Although the R1224yd(Z) heat flux is greater than that of R123 for all measured superheats, the R1336mzz(E) and the R123 boiling curves cross at a superheat of roughly 1.6 K. For superheats less than 1.6 K, the R1336mzz(E) heat flux is approximately 47 % greater than that of R123. Conversely, for superheats greater than 1.6 K, the R1336mzz(E) heat flux is approximately 19 % less than that of R123.

For a more detailed comparison, Fig. 7 plots the ratio of the R1336mzz(E) heat flux and the R1224yd(Z) heat flux to that of R123 at a saturation temperature of 277.6 K and at the same wall superheat. As done for Fig. 5, the heat flux ratio is shown as a solid line with dashed lines representing the 95 % multi-use confidence level for each mean. The largest heat flux ratio occurred at the lowest heat flux, while the smallest heat flux ratio was seen for the highest heat fluxes. The maximum and minimum heat flux ratios for R1336mzz(E) were  $3.07 \pm 0.03$  at  $10 \text{ kWm}^{-2}$  and  $1.15 \pm 0.03$  at  $79.4 \text{ kWm}^{-2}$ , respectively. The maximum and minimum heat flux ratios for R1224yd(Z) were  $2.03 \pm 0.03$  at  $10 \text{ kWm}^{-2}$  and  $0.82 \pm 0.01$  at  $100 \text{ kWm}^{-2}$ , respectively. The average heat flux ratio between  $10 \text{ kWm}^{-2}$  and  $80 \text{ kWm}^{-2}$  was approximately 1.13 and 1.57 for R1336mzz(E) and for R1224yd(Z), respectively. The average heat flux ratio between  $10 \text{ kWm}^{-2}$  and  $30 \text{ kWm}^{-2}$  was approximately 1.52 and 2.14 for R1336mzz(E) and for R1224yd(Z), respectively. Figure 7 illustrates the same waning benefit of the passive boiling enhancement for increasing heat flux as was shown in Fig. 5.

## COMPARISON TO POOL BOILING MODEL

The following provides a comparison of the present pool boiling measurements to a model developed by Kedzierski et al. (2018) and revised by Kedzierski and Lin (2019a). The pool boiling model predicts both mixed and single component refrigerants. The total boiling heat flux ( $q''$ ) of the composite model is based on a sum of the boiling phase-change heat flux and the heat flux due to single-phase convection:

$$q'' = 1.06 \times 10^8 \left( \frac{\sigma}{h_{fg} \rho_v r_c} \right)^{0.28} \Delta T_s^{\frac{29.3}{\text{Pr}_v^3 \sqrt{\text{Re}}}} \left( 1 - \frac{1.24 \Delta T_g}{\Delta T_s \frac{29.3}{\text{Pr}_v^3 \sqrt{\text{Re}}}} \right) \left( 1 - \frac{\Delta T_g}{\Delta T_s} \right)^{\frac{29.3}{\text{Pr}_v^3 \sqrt{\text{Re}}}} \left[ h_{fg} \rho_v \left( \frac{\sigma}{g(\rho_l - \rho_v)} \right)^{3/2} + 0.1 \frac{\mu_l^2 c_{pl} \text{Re}^{1.39}}{g(\rho_l - \rho_v)} \Delta T_s \right] \quad (1)$$

Equation (1) is a function of the temperature glide ( $\Delta T_g$ ), which is the difference between the dew-point temperature ( $T_d$ ) and the bubble-point temperature ( $T_b$ ). The temperature glide is zero for single component refrigerants. Consequently, the two terms in eq. (1) that account for the loss of available superheat and the mass transfer resistance, respectively, reduce to one for single component refrigerants where  $\Delta T_g = 0$ .

The first mixture effect term, the heat flux as degraded by the loss of available superheat ( $q_g''$ ), was modeled by Kedzierski et al. (2018) as:

$$\frac{q_g''}{q''} = \left( 1 - \frac{\Delta T_g}{\Delta T_s} \right)^{\frac{29.3}{Pr_l^3 \sqrt{Re}}} \quad (2)$$

where the temperature glide is normalized by the liquid superheat ( $\Delta T_s$ ). As defined by Shock (1982), the  $\Delta T_g$  is not available for boiling, which causes a boiling degradation because the superheat must surpass  $\Delta T_g$  before boiling can occur.

The second mixture effect term, the heat flux as degraded by the mass transfer resistance ( $q_d''$ ), was estimated by Kedzierski et al. (2018) as:

$$\frac{q_d''}{q''} = \left( 1 - \frac{1.24 \Delta T_g}{\Delta T_s \frac{29.3}{Pr_l^3 \sqrt{Re}}} \right) \quad (3)$$

As previously stated, eqs (2) and (3) are both equal to one for single component refrigerants and are included in eq. (1) as multipliers on the boiling model for mixed and pure refrigerants.

The refrigerant properties given in eq. (1) are the latent heat of vaporization ( $h_{fg}$ ), the vapor density ( $\rho_v$ ), the liquid density ( $\rho_l$ ), the surface tension ( $\sigma$ ), the liquid viscosity ( $\mu$ ), and the liquid specific heat ( $c_{pl}$ ). The  $g$  is the gravitational acceleration constant. In addition,  $r_c$  is the effective cavity radius for the Turbo-ESP surface, which is 2.67  $\mu\text{m}$ . Implicit in eq. (1) is that the value of  $r_c$  is fixed and that the refrigerant contact angle is 35°. The derivation of eq. (1), which is presented in Kedzierski and Lin (2019a), may be redone for different values of  $r_c$  and the contact angle in order to predict surfaces other than the Turbo-ESP and fluids other than refrigerants.

The bubble Reynolds number ( $Re$ ), based on the Stokes (1880) velocity and the Fritz (1935) equation for the bubble diameter ( $D_b$ ), was calculated by Kedzierski et al. (2018) for use in eq. (1) as:

$$Re = \frac{\rho_l u D_b}{\mu_l} = \frac{0.0214 \rho_l \sigma}{\mu_l^2} \sqrt{\frac{\sigma}{(\rho_l - \rho_v) g}} \quad (4)$$

The  $Re$  relates to the speed of the bubble leaving the surface. Bubbles that quickly leave the surface are not available to interact with other bubbles, i.e., to coalesce and improve boiling.

In addition, for smaller bubble  $Re$ , the bubble has a longer residence time on the boiling surface, which improves vapor seeding by increasing the instantaneous, local vapor quality. Consequently, smaller  $Re$  improves boiling.

The  $Pr_v$  is the dimensionless vapor Prandtl number:  $c_{pv} \mu_v / k_v$ . The  $Pr_v$  represents the ferocity of the boiling where smaller  $Pr_v$  correspond to greater energy diffusion as compared to momentum diffusion, i.e., more bubble nucleation as compared to liquid superheat. Because the  $Pr_v$  is cubed in eq. (1), while  $Re$  is given as a square root, the effect of  $Re$ , on a percentage basis, is significantly smaller than that of  $Pr_v$ . However, the range of  $Pr_v$  is generally limited to between 0.60 and 0.95, while the range of  $Re$  is not as bounded. Consequently, the effect of  $Re$  is not insignificant as compared to  $Pr_v$  as the powers to which each parameter is raised might suggest.

Figure 8 compares eq. (1) to the pool boiling measurements for the single component refrigerants R1336mzz(E) and R1224yd(Z). For the entire heat flux test range, the superheats for R1336mzz(E) and R1224yd(Z) were predicted to within  $\pm 0.45$  K. On average, the predicted heat flux differed from the measured values by - 12 % and - 17 % for R1336mzz(E) and R1224yd(Z), respectively. Larger percent deviations in the heat flux occur for the lowest test heat fluxes. Consequently, for superheats greater than 1.5 K, the average deviation between the measured and predicted heat flux was - 8 % and + 4 % for R1336mzz(E) and R1224yd(Z), respectively. Table 7 shows the fluid properties that were used to predict the boiling heat flux for R1336mzz(E) and R1224yd(Z). Table 7 shows fluid properties that were obtained from REFPROP 10.0 (Lemmon, et al., 2018) using the default equation of state. Due to limited data, an updated fluid file for R1224yd(Z) (Huber, 2020), that is not available in the public version of REFPROP 10.0 (Lemmon, et al., 2018), was used to predict the R1224yd(Z) properties. Similarly, an updated fluid file for R1336mzz(E) was obtained from Akasaka (2020) and Huber (2020). It is expected that the boiling heat transfer predictions for these fluids will change slightly as more fluid property data becomes available.

Figure 9 compares the measured heat flux for the R514A mixture at two different saturation temperatures to the boiling heat flux predicted with eq. (1). For the entire heat flux test range, the superheats for R514A were predicted to within  $\pm 0.7$  K. On average, the R514A predicted heat flux differed from the measured heat flux by - 4 % and + 4 % for 298.2 K and 277.6 K, respectively. The best predictions were made between 1 K and 2 K where the average deviation between the measured and predicted R514A heat flux was + 1 % and - 1 % for 298.2 K and 277.6 K, respectively. Table 7 shows the fluid properties that were used to predict the boiling heat flux for R514A were obtained using an updated fluid file from Huber (2020). In addition, the temperature glides were obtained from a linear weighted average of the Huber (2020) predictions and those obtained from Chemours (2019). As noted for the previous two fluids, it is expected that the boiling heat transfer predictions for R514A will change slightly as more fluid property data becomes.

Figure 10 illustrates the effect of two of the key fluid parameters on the heat flux as predicted by the pool boiling model. Figure 10 plots the percent change (referenced to the minimum heat flux) in the boiling heat flux as a function of both  $h_{fg} \rho_v$  and  $Pr_v$ . The significance of  $h_{fg} \rho_v$  is that it is the ebullition part of the boiling heat flux. The practical ranges of the property

values for  $h_{fg} \rho_v$  and  $Pr_v$  are used, which correspond to the range of a larger data set given in Kedzierski and Lin (2019a). The lower and upper abscissa of Fig. 10 plot the  $h_{fg} \rho_v$  and  $Pr_v$ , respectively. As immediately apparent, the  $h_{fg} \rho_v$  has a larger influence on the heat flux as compared to  $Pr_v$  where a roughly 150 % change in  $h_{fg} \rho_v$  through its entire range (0.4 MJ m<sup>-3</sup> to 1.0 MJ m<sup>-3</sup>) produces a roughly 110 % increase in the heat flux. In comparison, a 15 % decrease in  $Pr_v$  gives an approximate 50 % increase in the boiling heat flux. Consequently, the  $Pr_v$  is mathematically a stronger governing parameter of the heat flux than  $h_{fg} \rho_v$ ; however, due to the smaller practical range of  $Pr_v$  as compared to  $h_{fg} \rho_v$ , the  $Pr_v$  has a smaller influence.

Open symbols in Fig. 10, representing the properties of the examined test fluids taken from Table 7, more clearly illustrate the influence of properties on the relative performance of the fluids, as previously stated in the Experimental Results Section. For example, the larger heat flux of R1336mzz(E) as compared to that of R123 can be seen as a result of the two fluids having very similar  $Pr_v$  (within 5 %), but a larger difference in  $h_{fg} \rho_v$ . Here, the  $h_{fg} \rho_v$  for R1336mzz(E) is approximately twice that of R123, which causes R1336mzz(E) to generally have a larger heat flux. Conversely, R514A at both saturation temperatures have a  $h_{fg} \rho_v$  that is less than that of R123, while generally having larger heat fluxes (for the same superheat) as compared to R123 due to R514A's  $Pr_v$  being roughly 5 % larger than that of R123. R1224yd(Z) has larger heat fluxes as compared to R123 because its  $h_{fg} \rho_v$  is 60 % larger and its  $Pr_v$  is within 5 %.

## CONCLUSIONS

The pool boiling performance of a R1224yd(Z), R514A, and R1336mzz(E) on a flattened, horizontal Turbo-ESP surface was investigated. R1224yd(Z), R514A, and R1336mzz(E) are replacements for R123 and R245fa. The average heat flux ratio, as based on R123 performance, between 10 kWm<sup>-2</sup> and 80 kWm<sup>-2</sup> was approximately 1.13 and 1.57 for R1336mzz(E) and for R1224yd(Z), respectively. The average heat flux ratio between 10 kWm<sup>-2</sup> and 30 kWm<sup>-2</sup> was approximately 1.52 and 2.14 for R1336mzz(E) and for R1224yd(Z), respectively. The average heat flux ratio, as based on R123 performance, for R514A between 10 kWm<sup>-2</sup> and 80 kWm<sup>-2</sup> was approximately 1.43 and 1.30 for saturation temperatures of 298.2 K and 277.6 K, respectively. The average heat flux ratio for R514A between 10 kWm<sup>-2</sup> and 30 kWm<sup>-2</sup> was approximately 1.93 and 1.78 for saturation temperatures of 298.2 K and 277.6 K, respectively.

A previously developed prediction model for pure and mixture pool boiling of refrigerants on the Turbo-ESP surface was compared to the measurements. The model predicted the measured superheats of the mixed refrigerants and the single component refrigerants to within  $\pm 0.7$  K and  $\pm 0.45$  K, respectively. The model was used to show that the vapor Prandtl number and the product of the latent heat and vapor density significantly influence the boiling heat flux. The model is general enough to be used to predict surfaces other than the Turbo-ESP and fluids other than refrigerants by deriving the appropriate values for the effective surface radius and the contact angle.

## **ACKNOWLEDGEMENTS**

This work was funded by the National Institute of Standards and Technology (NIST). Thanks go to L. Cremaschi of Auburn University and to B. Dougherty of NIST. Furthermore, the author extends appreciation to A. Heckert of the NIST Statistical Engineering Division for his consultations on the uncertainty analysis. In-kind donations of the test refrigerants by K. Kontomaris of Chemours are greatly appreciated.

## NOMENCLATURE

### English Symbols

$A_n$	regression constant in Table 4 $n=0,1,2,3$
$c_p$	specific heat of fluid, $\text{J kg}^{-1} \text{K}^{-1}$
$D_b$	bubble diameter, m
$g$	gravitational acceleration constant, $9.8 \text{ m s}^{-2}$
$h_{fg}$	latent heat of vaporization, $\text{kJ kg}^{-1}$
$L$	test surface length shown in Fig. 3, m
$P$	pressure, Pa
$Pr_v$	dimensionless vapor Prantdl number, $c_{pv} \cdot \mu_v / k_v$
$q''$	average wall heat flux based on projected area, $\text{W} \cdot \text{m}^{-2}$
$q_d''$	heat flux degraded by the mass transfer resistance, $\text{W} \cdot \text{m}^{-2}$
$q_g''$	heat flux degraded by the loss of available superheat, $\text{W} \cdot \text{m}^{-2}$
$T$	temperature, K
$U$	expanded uncertainty
$V$	volume, $\text{m}^3$
$X$	model terms given in Table 1

### Greek symbols

$\Delta q''$	change in boiling heat flux, $\text{W} \cdot \text{m}^{-2}$
$\Delta T_g$	temperature glide: $T_d - T_b$ , K
$\Delta T_s$	wall superheat: $T_w - T_s$ , K
$\theta$	contact angle, degrees
$\mu$	dynamic viscosity, $\text{kg} \cdot \text{m}^{-1} \cdot \text{s}^{-1}$
$\sigma$	surface tension of refrigerant, $\text{N} \cdot \text{m}^{-1}$
$\rho$	density, $\text{kg} \cdot \text{m}^{-3}$

### English Subscripts

d	diffusion or dew point
b	bubble or bubble point
g	glide
l	liquid refrigerant
m	mixture
$q''$	heat flux
s	saturated state, streaming
w	wall temperature
v	refrigerant vapor

## REFERENCES

- Akasaka, R. 2020. Private Communication. Kyushu Sangyo University, Fukuoka Japan.
- Alam, J., Yamaguchi, K. Hori, Y., Kariya, K., and Miyara, A. 2019. Measurement of thermal conductivity and viscosity of cis-1-chloro-2,3,3,3-tetrafluoropropene (R-1224yd(Z)), Int. J. Refrigeration, 104, 221-228.
- Belsley, D. A., Kuh, E., and Welsch, R. E. 1980. Regression Diagnostics: Identifying Influential Data and Sources of Collinearity, New York: Wiley.
- Darabi, J.D., Ohadi, M.M., Fanni, M.A., Dessiatoun, S.V., and Kedzierski, M.A. 1999. Effect of Heating Boundary Conditions on Pool Boiling Experiments, *HVAC&R Research*, 5(4), 283-296.
- EU. 2014. Regulation (Eu) No 517/2014 of the European Parliament and of the Council of 16 April 2014 on fluorinated greenhouse gases and repealing Regulation (EC) No 842/2006, Official Journal of the European Union, L 150/195, <http://data.europa.eu/eli/reg/2014/517/oj>.
- Fritz, W. 1935. Berechnung des Maximalvolumen von Dampfblasen, Physikalische Zeitschrift, 36, 379-388.
- Gorgy, E. 2016. Nucleate boiling of low-GWP refrigerants on highly enhanced tube surface, Int. J. Heat Mass Transfer, 96, 660–6. <https://doi.org/10.1016/j.ijheatmasstransfer.2016.01.057>
- Huber, M. 2020. Private Communications. National Institute of Standards and Technology, Boulder, CO.
- Kaul, M. P., Kedzierski, M. A., and Didion, D. A. 1996. Horizontal Flow Boiling of Alternative Refrigerants within a Fluid Heated Micro-Fin Tube, *Process, Enhanced, and Multiphase Heat Transfer: A Festschrift for A. E. Bergles*, Editors: R. M. Manglik and A.D. Kraus, Begell House, Inc., New York, 167-173.
- Kedzierski, M. A., and Lin, L. 2020a. Pool Boiling of R515A, R1234ze(E), and R1233zd(E) on a Reentrant Cavity Surface,” International Journal of Heat and Mass Transfer, 161, <https://doi.org/10.1016/j.ijheatmasstransfer.2020.120252>
- Kedzierski, M. A., and Lin, L. 2020b, Effect of IF-WS2 Nanolubricant on R134a Boiling on a Reentrant Cavity Surface,” in press I. J. Trans. Phenomena
- Kedzierski, M. A., and Lin, L. 2019. Pool Boiling of HFO-1336mzz(Z) on a Reentrant Cavity Surface, International Journal of Refrigeration, 104, 476-483, [doi.org/10.1016/j.ijrefrig.2019.02.022](https://doi.org/10.1016/j.ijrefrig.2019.02.022)
- Kedzierski, M. A., Lin, L., and Kang, D. Y. 2018. Pool Boiling of Low GWP Replacements for R134a on a Reentrant Cavity Surface, J. Heat Transfer, 140(12), doi:10.1115/1.4040783.

Kedzierski, M. A., and Lin, L. 2018, Effect of IF-WS2 Nanolubricant on R134a Boiling on a Reentrant Cavity Surface; Extensive Measurement and Analysis Details,” NIST Technical Note 2033, U.S. Department of Commerce, Washington, D.C. <https://doi.org/10.6028/NIST.TN.2033>

Kedzierski, M. A. 2002. Use of Fluorescence to Measure the Lubricant Excess Surface Density During Pool Boiling, Int. J. Refrigeration, 25, 1110-1122.

Kedzierski, M. A. 2001. Use of Fluorescence to Measure the Lubricant Excess Surface Density During Pool Boiling, NISTIR 6727, U.S. Department of Commerce, Washington, D.C.

Kedzierski, M. A. 1999. Ralph L. Webb: A Pioneering Proselytizer for Enhanced Heat Transfer, J. Enhanced Heat Transfer, 6(2-4), 71-78.

Kedzierski, M. A. 1995. Calorimetric and Visual Measurements of R123 Pool Boiling on Four Enhanced Surfaces, NISTIR 5732, U.S. Department of Commerce, Washington.

Kondou, C., Higashi, Y., and Iwasaki, S. 2019. Surface Tension and Parachor Measurement of Low-Global Warming Potential Working Fluid cis-1-Chloro-2,3,3,3-tetrafluoropropene (R1224yd(Z)), J. Chem. Eng. Data, 64, 5462–5468.

Kontomaris, K. 2019. Private Communications. Chemours, Wilmington, DE.

Lemmon, E. W., Bell, I. H., Huber, M. L., and McLinden, M. O. 2018. *NIST Standard Reference Database 23 (REFPROP), Version 10.*, National Institute of Standards and Technology, Boulder, CO.

Longo, G.A., Mancin, S., Righetti, G., Zilio, C. 2019. R1224yd(Z) flow boiling inside a mini microfin tube, in: Proceedings of the 25th IIR International Congress of Refrigeration. Montréal, Canada.

Montreal Protocol. 1987. *Montreal Protocol on Substances that Deplete the Ozone Layer*. United Nations (UN), New York, NY, USA (1987 with subsequent amendments).

Myhre, G., D. Shindell, F.-M. Bréon, W. Collins, J. Fuglestedt, J. Huang, D. Koch, J.-F. Lamarque, D. Lee, B. Mendoza, T. Nakajima, A. Robock, G. Stephens, T. Takemura and H. Zhang. 2013. Anthropogenic and Natural Radiative Forcing Supplementary Material. In: *Climate Change 2013: The Physical Science Basis. Contribution of Working Group I to the Fifth Assessment Report of the Intergovernmental Panel on Climate Change* [Stocker, T.F., D. Qin, G.-K. Plattner, M. Tignor, S.K. Allen, J. Boschung, A. Nauels, Y. Xia, V. Bex and P.M. Midgley (eds.)]. Available from [www.climatechange2013.org](http://www.climatechange2013.org) and [www.ipcc.ch](http://www.ipcc.ch).

Peng, D. Y., and Robinson, D. B. 1976. A New Two-Constant Equation of State. Industrial and Engineering Chemistry: Fundamentals. 15, 59–64. doi:10.1021/i160057a011.

Rogers, J. S. 1961. Study of Low-Fin Tube 1929-1960, Wolverine Tube, Inc, Internal Report Neshan-1, p. 8.

Stokes, G. G. 1880. Mathematical and Physical Papers, 1, Cambridge University Press, London, 1880

Tokuhashi, K., Uchimaru, T., Takizawa, K., Kondo, S. 2018. Rate Constants for the Reactions of OH Radical with the ( E )/( Z ) Isomers of  $\text{CF}_3\text{CF}=\text{CHCl}$  and  $\text{CHF}_2\text{CF}=\text{CHCl}$ . <https://doi.org/10.1021/acs.jpca.7b11923>

UNEP. 2016. Amendment to the Montreal Protocol on Substances that Deplete the Ozone Layer, Kigali, 15 October 2016. <https://treaties.un.org/doc/Publication/CN/2016/CN.872.2016-Eng.pdf> (accessed July 25, 2017).

Webb, R. L. 1972. Heat Transfer Surface Having a High Boiling Heat Transfer Coefficient, US patent 3,696,861.

World Meteorological Organization (WMO). 2018. Scientific Assessment of Ozone Depletion, Report No. 58, WMO, Geneva, Switzerland.

**Table 1 Conduction model choice**

$X_0 = \text{constant (all models)}$ $X_1 = x$ $X_2 = y$ $X_3 = xy$ $X_4 = x^2 - y^2$ $X_5 = y(3x^2 - y^2)$ $X_6 = x(3y^2 - x^2)$ $X_7 = x^4 + y^4 - 6(x^2)y^2$ $X_8 = yx^3 - xy^3$	
Fluid	Most frequent models
R514A, $T_s = 298.2$ K $0.3 \text{ K} \leq \Delta T_s \leq 2.7 \text{ K}$	$X_1, X_2, X_5$ (165 of 201) 82 % $X_1, X_3, X_7, X_8$ (8 of 201) 4 %
R514A, $T_s = 277.6$ K $0.6 \text{ K} \leq \Delta T_s \leq 2.8 \text{ K}$	$X_1, X_2, X_5$ (171 of 297) 57 % $X_1, X_3$ (37 of 297) 37 % $X_1, X_2, X_5, X_7$ (33 of 297) 11 % $X_1, X_3, X_7$ (26 of 297) 9 %
R1224yd(Z), $T_s = 277.6$ K $0.3 \text{ K} \leq \Delta T_s \leq 2.3 \text{ K}$	$X_1, X_2, X_5$ (104 of 193) 54 % $X_1, X_3$ (32 of 193) 17 % $X_1, X_2, X_5, X_7$ (20 of 193) 11 % $X_1, X_3, X_7$ (17 of 193) 9 %
R1336mzz(E), $T_s = 277.6$ K $0.4 \text{ K} \leq \Delta T_s \leq 2.9 \text{ K}$	$X_1, X_2, X_5, X_7$ (41 of 114) 36 % $X_1, X_3, X_7$ (36 of 114) 31 % $X_1, X_2, X_4, X_5$ (15 of 114) 14 % $X_1, X_2, X_4, X_5, X_6, X_7$ (14 of 114) 13 %

**Table 2 Pool boiling data**

**R514A,  $T_s = 298.2$  K  
File: ESP14A2.dat**

$\Delta T_s$ (K)	$q''$ ( $Wm^{-2}$ )
3.02	107424.
3.00	107308.
2.76	99409.
2.77	99511.
2.53	93487.
2.54	93463.
2.38	87413.
2.39	87459.
2.21	81818.
2.22	81878.
2.05	76556.
2.04	76634.
1.90	71298.
1.91	71203.
1.80	66029.
1.79	65970.
1.67	60972.
1.64	60788.
1.47	56291.
1.48	56341.
1.42	50453.
1.43	50425.
1.33	44214.
1.33	44132.
1.21	37832.
2.62	100337.
2.63	100254.
2.43	93413.
2.40	93364.
2.20	85086.
2.22	85087.
2.02	76632.
2.03	76695.
1.81	68930.
1.81	68954.
1.60	61737.
1.60	61805.
1.42	55379.
1.42	55511.
1.22	48695.
1.23	48667.
1.14	41097.
1.13	41009.
0.98	33100.
0.97	32988.
0.76	25484.
0.76	25445.
0.51	19252.
0.50	19186.
0.32	13263.
2.65	100377.
2.65	100389.
2.44	91984.
2.45	91831.
2.21	84184.
2.22	84253.
2.02	76915.
2.06	76968.

1.82	69965.
1.82	70018.
1.67	63231.
1.66	63401.
1.56	55336.
1.54	55293.
1.40	46731.
1.41	46681.
1.12	39767.
1.15	39091.
0.88	32605.
0.88	32555.
0.64	26865.
0.61	26715.
0.48	20290.
0.49	20315.
0.33	13520.
2.60	99843.
2.62	99865.
2.46	93313.
2.45	93313.
2.26	84838.
2.25	84798.
2.04	77118.
2.04	77040.
1.86	69363.
1.89	69342.
1.68	61894.
1.71	61943.
1.49	55029.
1.50	55001.
1.34	47689.
1.33	47687.
1.17	40399.
1.16	40209.
0.96	33154.
0.96	33164.
0.76	26098.
0.75	26040.
0.53	19776.
0.52	19956.
0.35	13648.
2.59	99760.
2.58	99662.
2.42	91756.
2.42	91870.
2.24	83944.
2.24	83973.
2.07	73850.
2.04	73715.
1.79	66645.
1.80	66634.
1.57	60440.
1.55	60414.
1.37	55099.
1.37	55126.
1.18	49549.
1.18	49625.
1.07	41815.
1.05	41896.
0.89	34352.
0.90	34284.

0.69	27001.
0.69	26983.
0.54	20215.
0.53	20431.
0.36	13871.
2.72	96510.
2.70	96387.
2.45	88814.
2.46	88806.
2.23	81858.
2.23	81869.
2.07	75883.
2.07	76042.
1.87	69369.
1.85	69402.
1.70	62064.
1.69	62158.
1.52	54966.
1.51	54752.
1.29	47704.
1.30	47561.
1.17	42131.
1.17	41951.
0.94	33001.
0.91	32997.
0.71	25945.
0.71	25890.
0.51	19511.
0.50	19591.
0.33	13264.
2.68	98453.
2.70	97404.
2.45	90352.
2.45	90397.
2.26	83666.
2.24	83660.
2.11	75596.
2.09	75440.
1.86	68314.
1.89	68200.
1.68	61009.
1.68	61003.
1.50	53689.
1.49	53644.
1.30	46749.
1.31	46684.
1.10	40062.
1.11	40039.
0.93	32999.
0.91	33277.
0.72	25733.
0.76	25694.
0.55	19117.
0.54	19161.
0.37	12967.
2.71	96098.
2.73	95931.
2.49	89255.
2.47	89348.
2.26	83027.
2.27	83085.
2.10	75566.

2.08	75552.
1.96	68162.
1.94	67901.
1.78	59206.
1.78	59079.
1.51	51824.
1.49	51548.
1.25	45223.
1.24	45322.
1.03	39652.
1.06	39518.
0.86	33706.
0.87	33188.
0.75	25593.
0.75	25603.
0.57	18813.
0.57	18813.
0.42	12685.
0.39	12543.

**R514A,  $T_s = 277.6$  K**  
**File: ESP14A4.dat**

$\Delta T_s$ (K)	$q''$ (Wm <sup>-2</sup> )
2.99	94168.
2.99	94172.
2.85	87152.
2.77	87019.
2.53	79190.
2.52	79142.
2.27	72547.
2.25	72567.
2.10	67439.
2.07	67400.
1.93	61831.
1.90	61836.
1.78	56420.
1.74	56502.
1.53	49187.
1.53	49815.
1.32	43221.
1.35	43210.
1.10	37343.
1.11	37253.
0.99	32064.
0.98	32121.
0.78	25774.
0.77	25776.
0.77	25776.
2.90	89300.
2.85	89423.
2.72	84149.
2.72	83903.
2.52	79006.
2.50	78918.
2.34	73268.
2.35	73284.
2.19	68835.
2.22	68743.
1.99	63085.
1.98	62925.
1.77	57181.
1.79	57158.

1.59	52168.
1.62	52441.
1.45	47170.
1.39	49116.
1.29	42034.
1.32	42140.
1.00	30632.
0.99	30860.
0.83	24097.
0.84	24054.
0.58	18522.
2.95	89255.
2.95	89417.
2.77	83812.
2.74	83785.
2.59	78426.
2.58	78473.
2.47	73488.
2.44	73549.
2.23	68281.
2.19	68042.
2.06	63020.
2.08	62784.
1.82	55610.
1.81	55707.
1.55	50821.
1.60	48601.
1.35	43679.
1.39	41667.
1.17	35296.
1.23	35182.
1.04	30493.
1.05	30391.
0.84	24261.
0.82	24163.
0.70	17639.
2.63	87877.
2.66	87884.
2.52	82704.
2.49	82779.
2.35	77991.
2.39	78171.
2.25	72698.

2.24	72949.
2.07	67949.
2.06	67867.
1.85	62372.
1.87	62657.
1.61	55491.
1.67	55805.
1.45	49036.
1.44	48839.
1.27	41755.
1.26	41775.
1.08	35004.
1.08	34947.
0.91	30118.
0.91	30176.
0.77	23242.
0.76	23406.
0.50	17565.
3.00	87611.
2.99	87869.
2.70	82782.
2.70	82800.
2.51	77772.
2.53	78200.
2.39	72926.
2.43	72858.
2.18	67773.
2.20	67671.
1.98	62588.
2.01	62512.
1.75	55430.
1.71	55257.
1.52	48438.
1.54	48650.
1.28	41856.
1.27	44011.
1.12	35398.
1.11	35507.
0.96	30584.
0.93	30751.
0.83	25696.
0.77	27638.
0.68	17143.

2.84	88348.
2.83	88395.
2.67	83148.
2.63	82858.
2.49	78253.
2.49	77995.
2.30	73097.
2.30	73097.
2.15	67971.
2.15	67971.
1.96	62649.
1.98	62693.
1.74	55534.
1.74	55433.
1.53	48305.
1.52	48211.
1.29	41349.
1.28	41346.
1.10	34696.
1.10	34845.
0.89	32086.
0.94	30258.
0.75	24195.
0.75	24254.
0.57	18281.
2.59	87888.
2.58	87825.
2.39	83021.
2.44	82954.
2.25	78110.
2.24	78533.
1.99	71253.
2.02	71571.
1.89	66819.
1.89	66879.
1.74	61510.
1.72	61340.
1.59	56087.
1.58	56142.
1.35	48875.
1.35	48583.
1.13	41861.
1.13	42059.
0.92	35279.
0.92	35301.
0.76	30562.
0.77	30590.
0.60	24261.
0.58	24564.
0.47	17986.
2.58	90025.
2.56	89778.
2.41	84469.
2.41	84469.
2.18	75311.
2.18	75395.
2.01	68061.
2.02	68072.

1.84	62045.
1.83	62069.
1.63	54740.
1.63	54860.
1.40	47919.
1.45	48021.
1.14	41282.
1.14	41211.
1.04	34456.
1.04	34584.
0.84	27762.
0.84	27762.
0.71	21708.
2.54	89232.
2.55	89383.
2.43	83518.
2.42	83498.
2.19	77082.
2.23	77108.
2.03	71265.
2.00	71355.
1.83	65462.
1.82	65384.
1.66	60545.
1.66	60603.
1.46	54143.
1.48	54160.
1.24	47904.
1.28	48002.
1.11	41463.
1.09	41438.
0.93	34964.
0.96	34679.
0.89	29207.
0.87	29372.
0.71	22562.
0.72	22574.
0.50	16965.
2.73	89334.
2.73	89028.
2.57	83345.
2.56	83333.
2.37	77751.
2.38	77688.
2.22	72458.
2.24	72695.
2.06	67762.
2.03	67606.
1.92	62354.
1.91	62337.
1.68	55237.
1.68	55144.
1.50	47725.
1.50	47835.
1.24	40440.
1.21	42304.
1.14	34422.
1.09	34601.

0.92	30152.
0.89	30129.
0.84	23572.
0.81	23560.
0.58	16556.
2.62	89512.
2.62	89834.
2.49	83892.
2.50	83872.
2.35	78331.
2.41	78362.
2.16	72366.
2.20	72561.
2.00	65519.
1.94	65202.
1.77	60410.
1.74	60361.
1.60	55218.
1.58	55069.
1.42	48395.
1.42	48365.
1.18	41242.
1.16	41290.
1.02	34581.
1.04	34653.
0.81	28427.
0.81	28411.
0.69	23650.
0.68	23688.
0.52	17551.
2.55	90877.
2.61	88606.
2.41	82923.
2.39	85347.
2.24	77909.
2.24	77618.
2.10	72665.
2.09	72734.
1.95	67149.
1.95	66936.
1.79	60526.
1.78	60400.
1.64	55189.
1.63	55078.
1.48	47528.
1.47	47685.
1.24	40752.
1.24	40672.
1.05	34343.
1.07	34267.
0.94	29479.
0.93	29592.
0.78	23075.
0.75	23084.
0.62	16709.
0.62	16709.

R1224yd(Z),  $T_s = 277.6$  K  
 File: ESPyd.dat

$\Delta T_s$ (K)	$q''$ (Wm <sup>-2</sup> )
2.23	87965.
2.21	87740.
2.12	82838.
2.10	82657.
1.94	76450.
1.92	76428.
1.79	71246.
1.77	71133.
1.67	66577.
1.62	66205.
1.47	59946.
1.45	59955.
1.36	54113.
1.34	54156.
1.15	46880.
1.19	46920.
0.94	40379.
0.93	40398.
0.75	34797.
0.81	34864.
0.69	28354.
0.69	28386.
0.48	22036.
0.47	22074.
0.32	16785.
2.18	88691.
2.16	88711.
2.06	82445.
2.04	82200.
1.88	77088.
1.88	76985.
1.74	72176.
1.76	72456.
1.61	67163.
1.63	67351.
1.45	61855.
1.48	62196.
1.27	55066.
1.25	55003.
1.06	48752.
1.07	48789.
0.88	41890.
0.89	41999.
0.71	34712.
0.71	34870.
0.60	29412.
0.60	29314.
0.45	22209.
2.04	88476.
2.08	88522.
1.91	83360.
1.91	83360.
1.86	77956.
1.78	80387.
1.63	72614.
1.64	72687.
1.52	67410.
1.52	67810.
1.40	61674.
1.39	61892.

1.20	55302.
1.19	55372.
1.08	49454.
1.04	49577.
0.90	40403.
0.92	40185.
0.68	33882.
2.45	89426.
2.35	89111.
2.28	84106.
2.28	84169.
2.15	81110.
2.16	78746.
2.02	73622.
2.04	73495.
1.87	67818.
1.89	67748.
1.70	62455.
1.69	62458.
1.49	55941.
1.52	56145.
1.37	49222.
1.34	49260.
1.19	42068.
1.19	42146.
0.98	34906.
0.97	34958.
0.87	28835.
0.86	28664.
0.58	22442.
0.56	22408.
0.34	16922.
2.39	89516.
2.36	89055.
2.22	84529.
2.22	84495.
2.08	79522.
2.06	79338.
1.92	74914.
1.89	74835.
1.79	68983.
1.79	69090.
1.70	65550.
1.74	63506.
1.55	57307.
1.55	57297.
1.41	49808.
1.40	49723.
1.24	42129.
1.24	42115.
0.99	35591.
1.00	35496.
0.84	30899.
0.86	30796.
0.63	23210.
0.62	23105.
0.34	16549.
2.27	94906.
2.29	91900.
2.11	87010.
2.11	87010.
1.99	81678.
1.96	81341.
1.88	76200.
1.85	75610.

1.65	70354.
1.66	70020.
1.62	64729.
1.61	64668.
1.43	57400.
1.42	57419.
1.29	50905.
1.28	51029.
1.16	44448.
1.16	44264.
0.91	36076.
0.96	36162.
0.79	30656.
0.79	30689.
0.51	23579.
0.50	23571.
0.36	17472.
2.22	90295.
2.22	90474.
2.13	84394.
2.13	84145.
1.99	77565.
1.98	77468.
1.80	72191.
1.82	72416.
1.64	67589.
1.61	67886.
1.46	63208.
1.47	63290.
1.34	56121.
1.34	56135.
1.17	48911.
1.18	48916.
1.00	41532.
1.00	41489.
0.78	34601.
0.78	34655.
0.63	29994.
0.63	29929.
0.47	23585.
0.45	23715.
0.39	16788.
2.25	91770.
2.24	91702.
2.15	83967.
2.12	86942.
2.06	78892.
2.06	78964.
1.92	73272.
1.90	73198.
1.81	68125.
1.77	68144.
1.72	62358.
1.70	62427.
1.56	55543.
1.55	55547.
1.40	48969.
1.39	49008.
1.24	42245.
1.19	42146.
1.04	35273.
1.03	35252.
0.89	30117.
0.87	30021.
0.66	23376.

0.66	23304.
0.41	17622.
0.41	17579.

**R1336mzz(E),  $T_s = 277.6$  K**  
**File: ESPzze.dat**

$\Delta T_s$ (K)	$q''$ (Wm <sup>-2</sup> )
2.78	82030.
1.69	48842.
1.41	40307.
1.40	40243.
1.10	31416.
1.12	31321.
0.85	24698.
0.84	24606.
0.71	19047.
0.71	19004.
0.60	13546.
2.77	82067.
0.60	13530.
0.41	7260.
0.41	7245.
2.51	73842.
2.51	73746.
2.25	65351.
2.25	65345.
1.99	57237.
1.98	57210.
2.90	81313.
2.17	62455.
2.01	57610.
1.99	59827.
1.78	53104.
1.79	53044.
1.55	46267.
1.56	44222.
1.36	40495.
1.36	38494.
1.18	33950.
2.88	81297.
1.18	33908.
1.03	29342.
1.04	29310.
0.88	24824.
0.87	24796.
0.72	19327.
0.72	19252.
0.57	12733.
0.58	12704.
2.73	76313.
2.68	77436.
2.56	71123.
2.57	71168.
2.33	67775.
2.41	66148.
2.78	81863.
2.10	58511.
1.83	54749.
1.83	54723.
1.62	48085.
1.61	48092.

1.35	40572.
1.40	38159.
1.11	31722.
1.11	31697.
0.92	26028.
2.86	80224.
0.91	25982.
0.75	20555.
0.75	20507.
0.65	14949.
0.67	14570.
2.61	74958.
2.64	73736.
2.46	67457.
2.47	67353.
2.31	62566.
2.23	64085.
2.78	81547.
1.92	57613.
1.68	51077.
1.68	51063.
1.47	41800.
1.50	41327.
1.15	32396.
1.14	32355.
0.81	22581.
0.82	22489.
2.78	81500.
2.61	75454.
2.63	75091.
2.36	70844.
2.38	68481.
2.17	62145.
2.14	64347.
2.84	80437.
1.98	57590.
1.79	50729.
1.76	51161.
1.54	44834.
1.53	44734.
1.29	37718.
1.27	37853.
1.05	31491.
1.05	31421.
0.86	24758.
2.84	80413.
0.86	24765.
0.74	19183.
0.74	19128.
0.67	13758.
0.62	13909.
0.41	9324.
0.45	7458.
2.63	77206.
2.67	75740.
2.40	71448.
2.48	69555.
2.23	64391.
2.20	64742.
1.98	57666.

**Table 3 Number of test days and data points**

Fluid	Number of days	Number of data points/ Number of data points with outliers removed
R514A, $T_s = 298.2$ K $0.3 \text{ K} \leq \Delta T_s \leq 2.7 \text{ K}$	8	201/192
R514A, $T_s = 277.6$ K $0.6 \text{ K} \leq \Delta T_s \leq 2.8 \text{ K}$	12	297/285
R1224yd(Z), $T_s = 277.6$ K $0.3 \text{ K} \leq \Delta T_s \leq 2.3 \text{ K}$	8	193/192
R1336mzz(E), $T_s = 277.6$ K $0.4 \text{ K} \leq \Delta T_s \leq 2.9 \text{ K}$	5	114/109

**Table 4 Estimated parameters for cubic boiling curve fits**

$$\Delta T_s = A_0 + A_1 q'' + A_2 q''^2 + A_3 q''^3$$

$\Delta T_s$  in Kelvin and  $q''$  in  $\text{Wm}^{-2}$

Fluid	$A_0$	$A_1$	$A_2$	$A_3$
R514A, $T_s = 298.2$ K $0.3 \text{ K} \leq \Delta T_s \leq 2.7 \text{ K}$	-0.09337412	$3.412185 \times 10^{-5}$	$-1.326297 \times 10^{-10}$	$7.120032 \times 10^{-16}$
R514A, $T_s = 277.6$ K $0.6 \text{ K} \leq \Delta T_s \leq 2.8 \text{ K}$	0.2262807	$1.757428 \times 10^{-5}$	$2.016295 \times 10^{-10}$	$-9.016386 \times 10^{-16}$
R1224yd(Z), $T_s = 277.6$ K $0.3 \text{ K} \leq \Delta T_s \leq 2.3 \text{ K}$	-0.1897407	$3.574567 \times 10^{-5}$	$-1.841726 \times 10^{-10}$	$9.993298 \times 10^{-16}$
R1336mzz(E), $T_s = 277.6$ K $0.4 \text{ K} \leq \Delta T_s \leq 2.9 \text{ K}$	0.3026826	$1.734880 \times 10^{-5}$	$2.905054 \times 10^{-10}$	$-1.456033 \times 10^{-15}$

**Table 5 Residual standard deviation of  $\Delta T_s$** 

Fluid	(K)
R514A, $T_s = 298.2$ K $0.3 \text{ K} \leq \Delta T_s \leq 2.7 \text{ K}$	0.06
R514A, $T_s = 277.6$ K $0.6 \text{ K} \leq \Delta T_s \leq 2.8 \text{ K}$	0.10
R1224yd(Z), $T_s = 277.6$ K $0.3 \text{ K} \leq \Delta T_s \leq 2.3 \text{ K}$	0.11
R1336mzz(E), $T_s = 277.6$ K $0.4 \text{ K} \leq \Delta T_s \leq 2.9 \text{ K}$	0.05

**Table 6 Average magnitude of 95 % multi-use confidence interval for mean  $\Delta T_s$** 

Fluid	$U$ (K)
R514A, $T_s = 298.2$ K $0.3 \text{ K} \leq \Delta T_s \leq 2.7 \text{ K}$	0.03
R514A, $T_s = 277.6$ K $0.6 \text{ K} \leq \Delta T_s \leq 2.8 \text{ K}$	0.04
R1224yd(Z), $T_s = 277.6$ K $0.3 \text{ K} \leq \Delta T_s \leq 2.3 \text{ K}$	0.05
R1336mzz(E), $T_s = 277.6$ K $0.4 \text{ K} \leq \Delta T_s \leq 2.9 \text{ K}$	0.03

**Table 7 Selected fluid properties of test refrigerants at saturation using REFPROP 10.0 default equations (Lemmon et al., 2018)**

Fluid	$T_s$ (K)	$P_v$ (kPa)	$Pr_v$ (-)	$\Delta T_g$ (K)	$\mu$ ( $\mu\text{kg}\cdot\text{m}^{-1}\cdot\text{s}^{-1}$ )	$\sigma$ ( $\text{N}\cdot\text{m}^{-1}$ )	$\rho_l$ ( $\text{kg}\cdot\text{m}^{-3}$ )	$\rho_v$ ( $\text{kg}\cdot\text{m}^{-3}$ )	$h_{fg}$ ( $\text{kJ}\cdot\text{kg}^{-1}$ )	$c_{pl}$ ( $\text{kJ}\cdot\text{kg}^{-1}\text{K}^{-1}$ )
R1224yd(Z) <sup>4</sup>	277.6	67.424	0.687 <sup>5</sup>	0.00	377.34	0.0152	1416.1	4.50	173.46	1.0941
R1336mzz(E) <sup>6</sup>	277.6	88.027	0.787	0.00	346.24	0.0122	1382.9	6.55	155.16	1.2165
R514A <sup>7</sup>	277.6	35.50 <sup>8</sup>	0.782	0.20 <sup>9</sup>	463.91	0.0211	1379.6	2.30	205.98 <sup>10</sup>	1.1599 <sup>10</sup>
R514A <sup>7</sup>	298.2	84.01 <sup>8</sup>	0.788	0.25 <sup>9</sup>	366.51	0.0183	1333.0	5.09	196.51 <sup>10</sup>	1.1861 <sup>10</sup>
R1336mzz(Z)	277.6	30.576	0.769	0.00	467.22	0.0182	1416.9	2.22	177.56	1.1784
R1336mzz(Z)	298.2	73.705	0.772	0.00	363.29	0.0155	1364.5	5.09	168.45	1.2208
R123	277.6	39.85	0.823	0.00	533.98	0.0177	1515.3	2.70	179.69	0.9953

<sup>4</sup> Updated REFPROP 10.0 fluid file from Huber (2020) using transport properties fitted to data from Alam et al. (2019) and Kondou et al. (2019)

<sup>5</sup> The  $Pr_v$  for R1224yd(Z) was calculated using the  $c_{pv}$  from REFPROP (Lemmon et al., 2018) and linear fits of the saturated measurements for the vapor thermal conductivity and the vapor viscosity from Alam et al. (2019).

<sup>6</sup> REFPROP 10.0 fluid file from Akasaka (2020) and Huber (2020).

<sup>7</sup> REFPROP 10.0 fluid file for R514A was obtained from Huber (2020).

<sup>8</sup> Vapor pressure measured in NIST pool boiling test apparatus

<sup>9</sup> Linear, weighted average of REFPROP 10.0 predictions with Huber (2020) and Chemours (2019).

<sup>10</sup> Linear average of REFPROP 10.0 predictions with Huber (2020) and Chemours (2019).

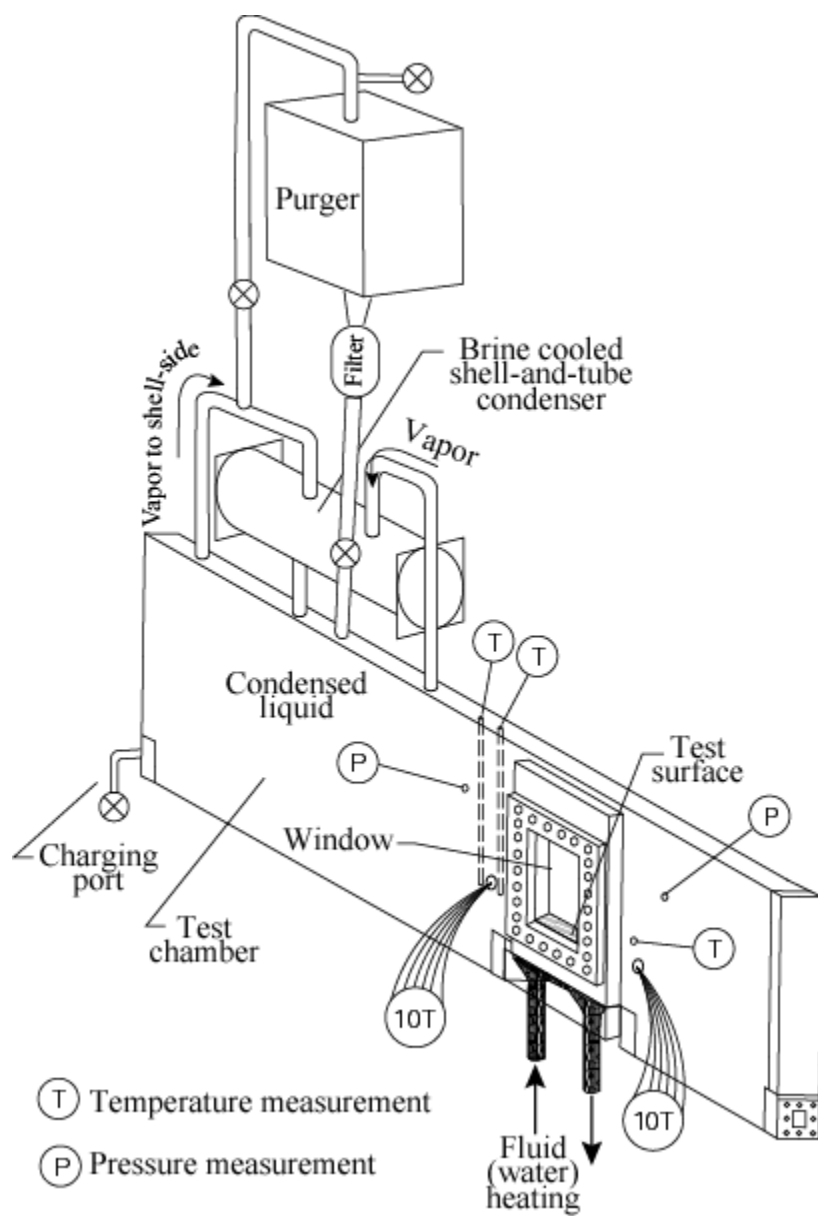


**Fig. 1 Schematic of test apparatus**

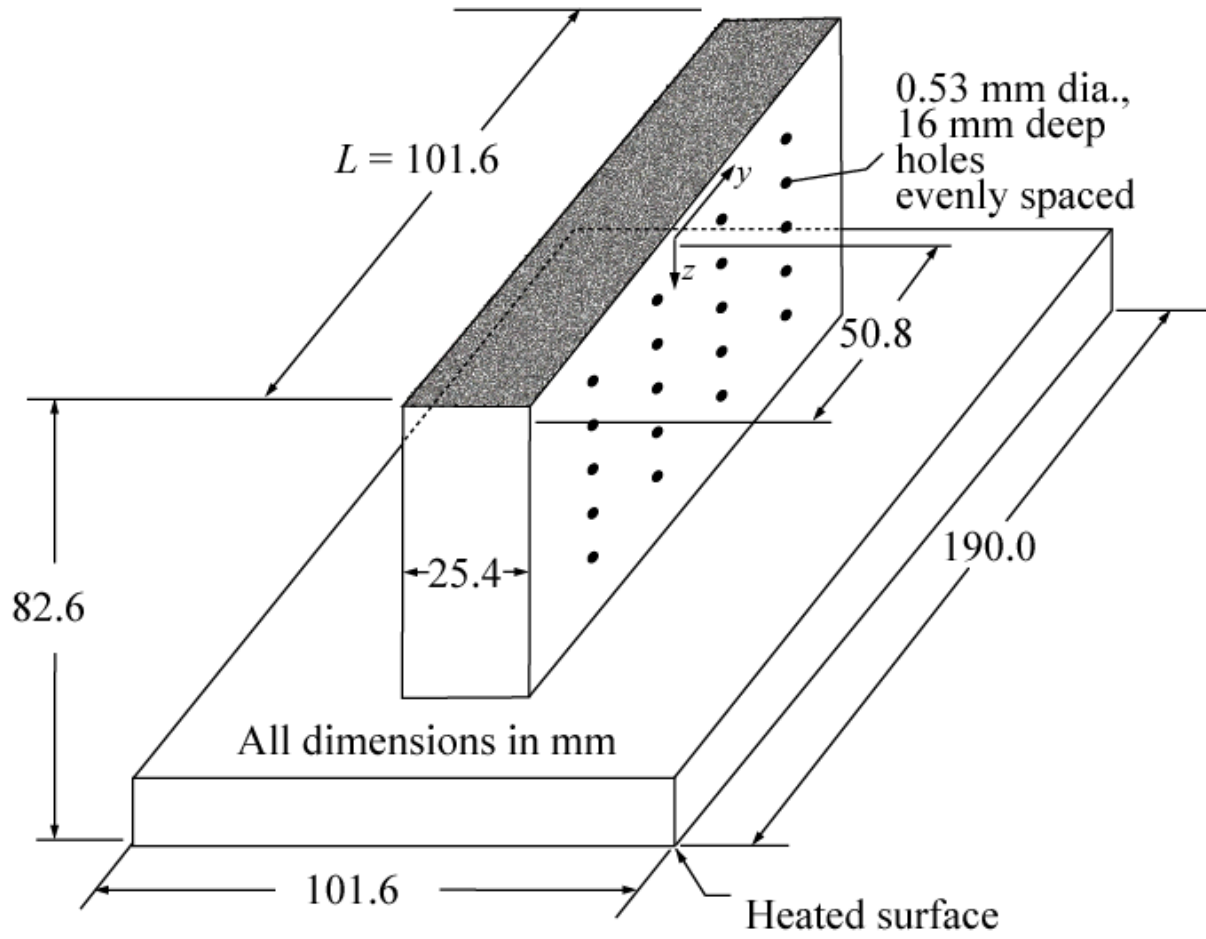


**Fig. 2 OFHC copper flat test plate with Turbo-ESP surface and thermocouple coordinate system**

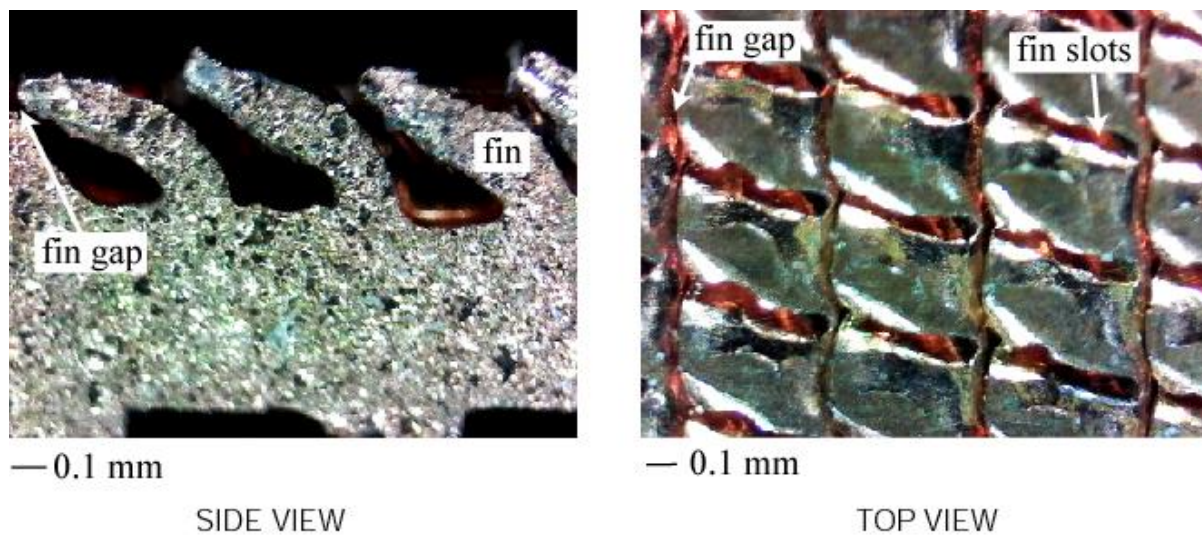


**Fig. 3 Photograph of Turbo-ESP surface**

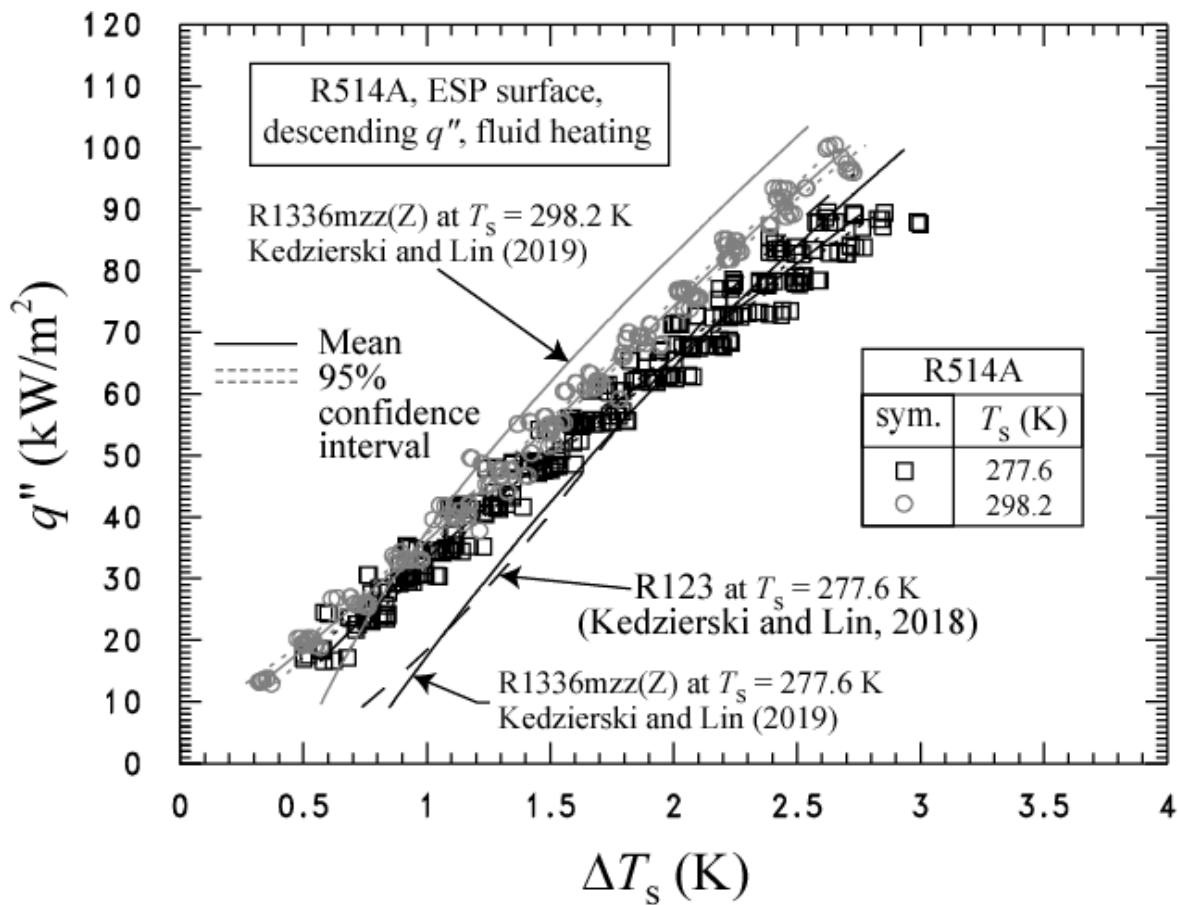


**Fig. 4 Comparison of boiling curves for R514A, and R1336mzz(Z) at 277.6 K and 298.2 K**

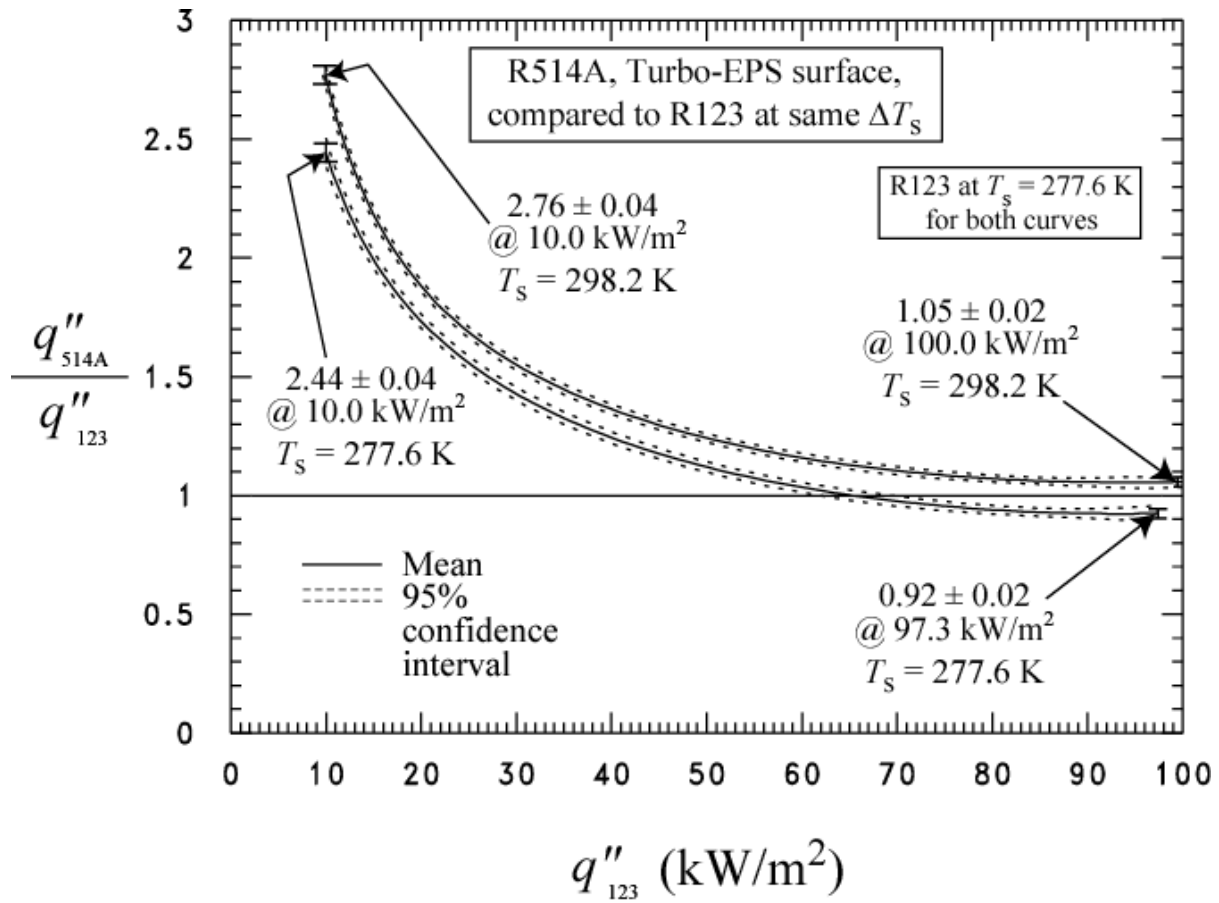


**Fig. 5 Comparison of R514A heat fluxes for different saturation temperatures to that for R123 at the same wall superheat**

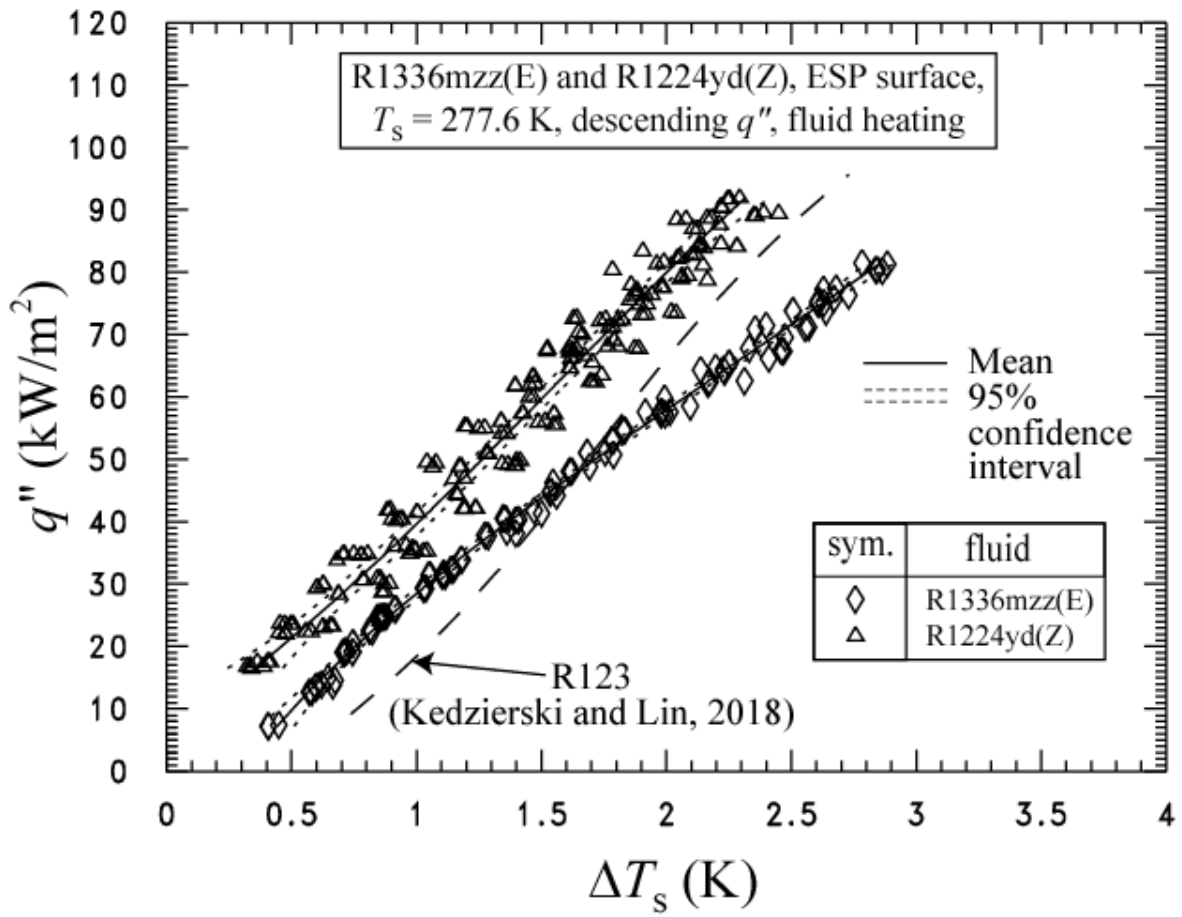


**Fig. 6** Comparison of boiling curves for R1336mzz(E) and R1224yd(Z) at 277.6 K

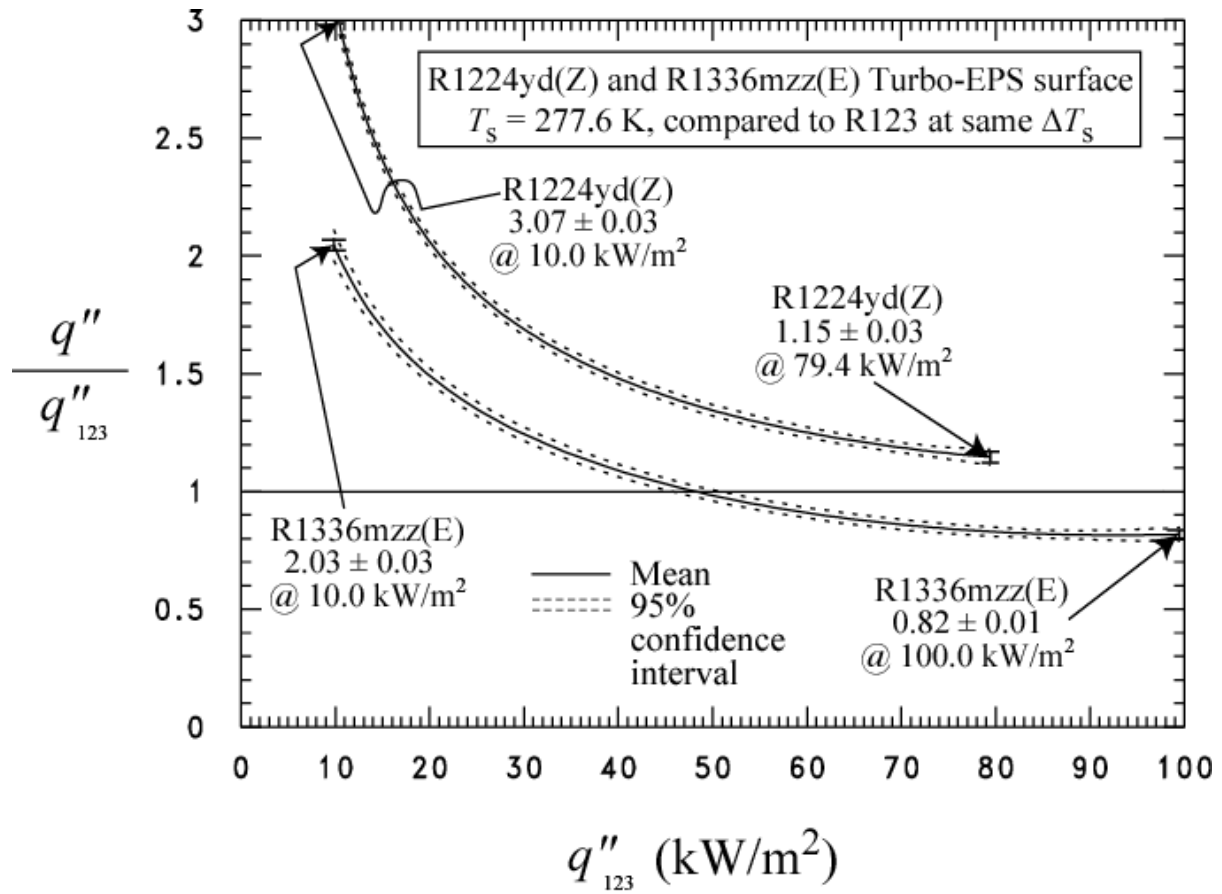


**Fig. 7 Comparison of R1224yd(Z) and R1336mzz(E) heat fluxes to that for R123 at the same wall superheat**

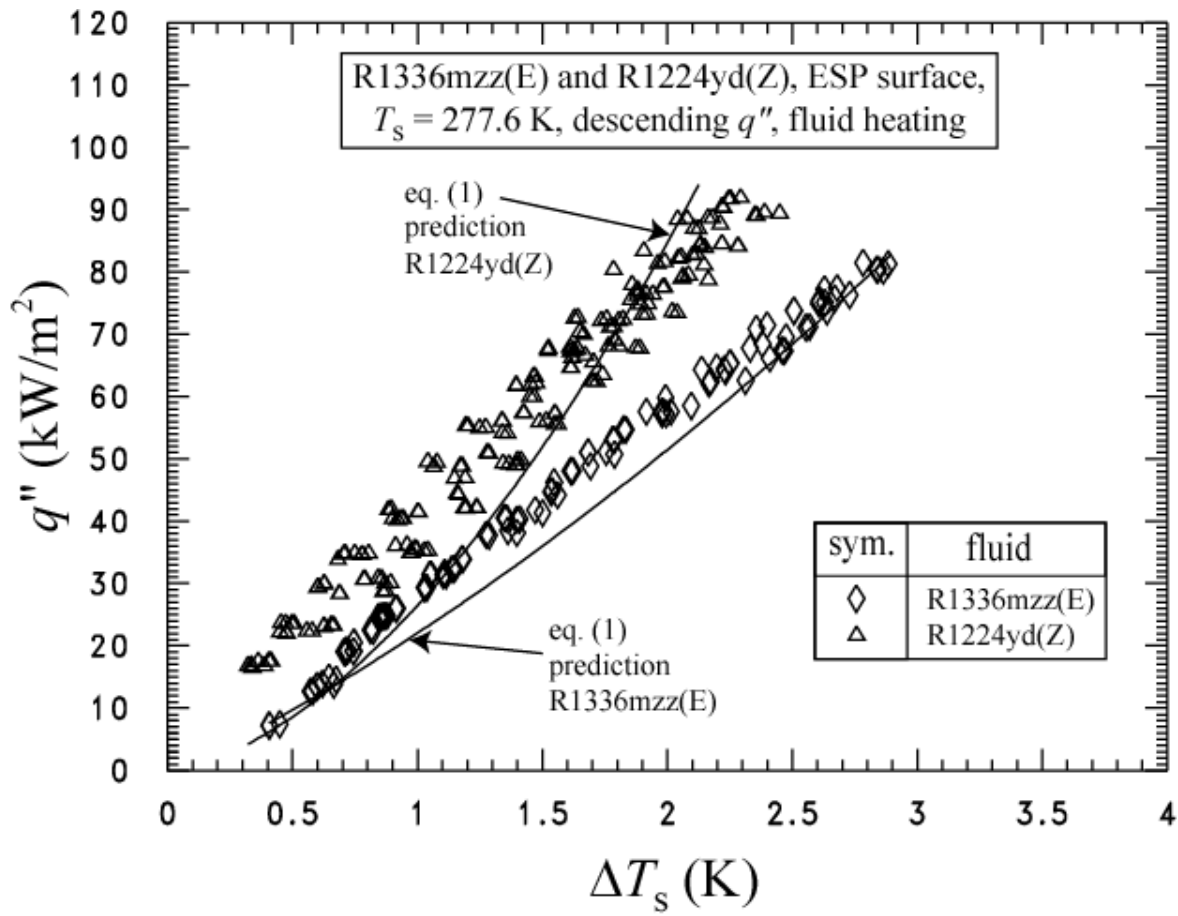


**Fig. 8 Comparison of pool boiling model for Turbo-ESP surface to present measurements for R1224yd(Z) and R1336mzz(E)**

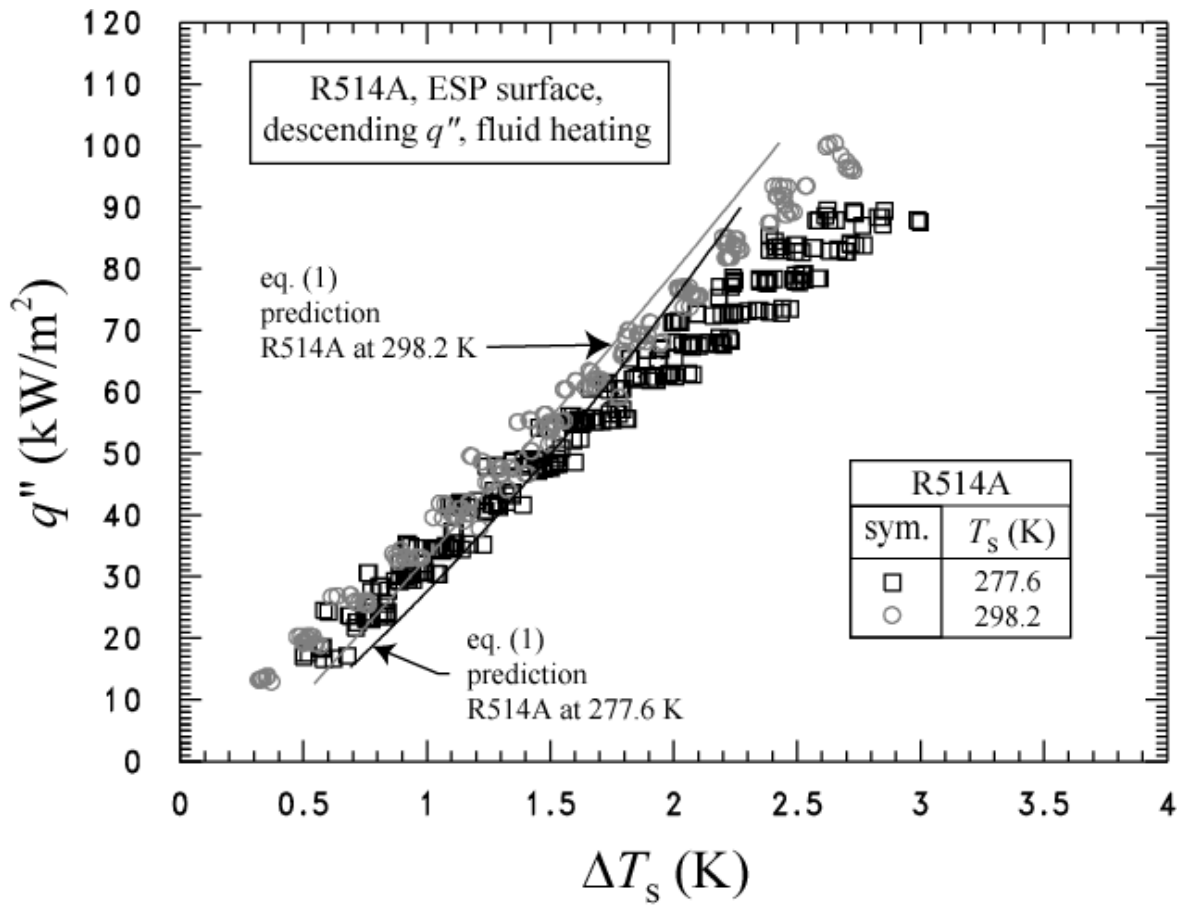


**Fig. 9 Comparison of refrigerant mixture pool boiling model for Turbo-ESP surface to R514A measurements**

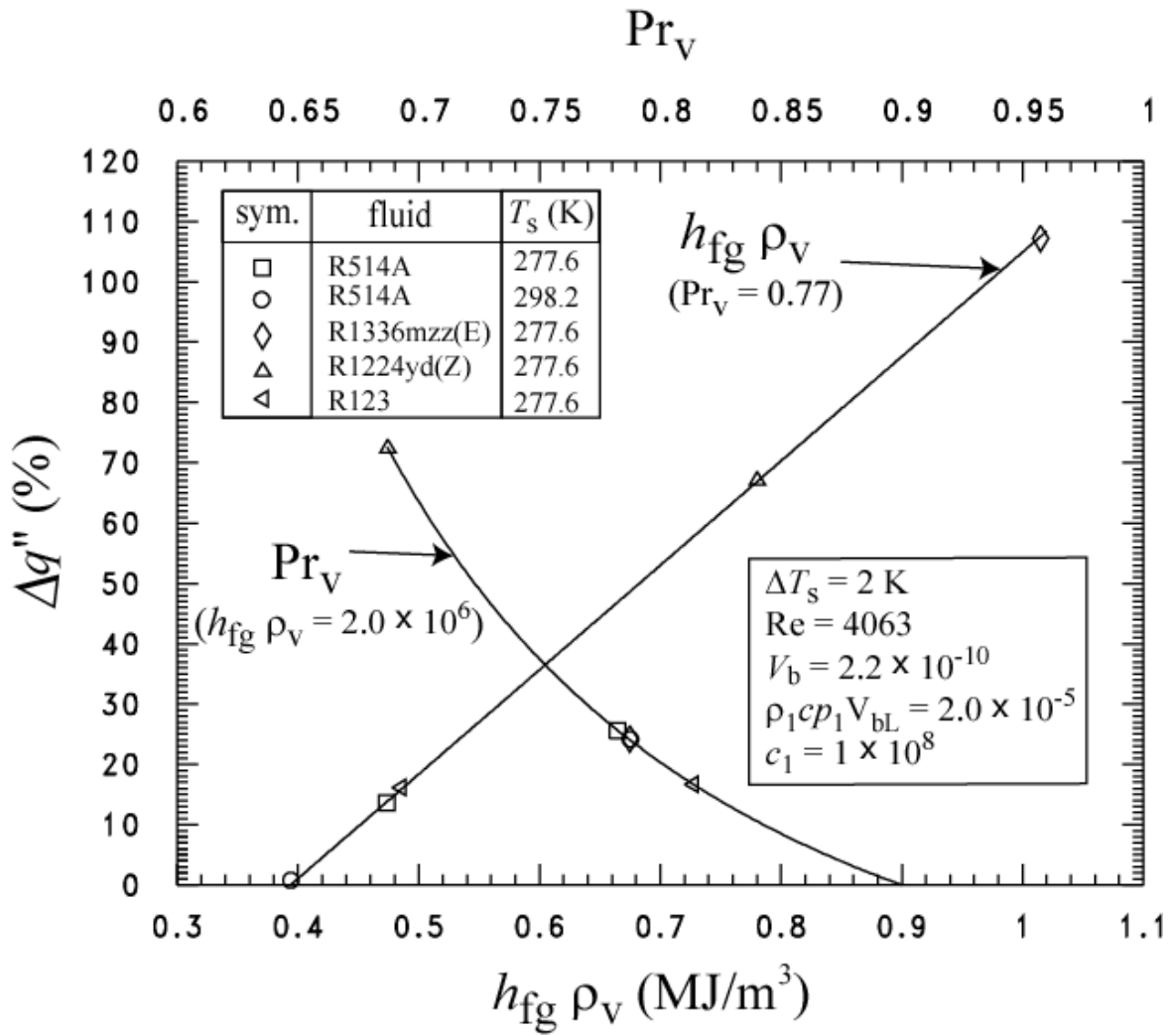


**Fig. 10** Illustration of effect of key properties on pool boiling model heat flux

### APPENDIX A: UNCERTAINTIES

Figure A.1 shows the expanded relative (percent) uncertainty of the heat flux ( $U_{q''}$ ) as a function of the heat flux. Figure A.2 shows the expanded uncertainty of the wall temperature as a function of the heat flux. The uncertainties shown in Figs. A.1 and A.2 are "within-run uncertainties." They do not include the uncertainties due to "between-run effects" or differences observed between tests taken on different days. The "within-run uncertainties" include only the random effects and uncertainties associated with one particular test. All other uncertainties reported in this study are "between-run uncertainties" which include all random effects such as surface past history or seeding.

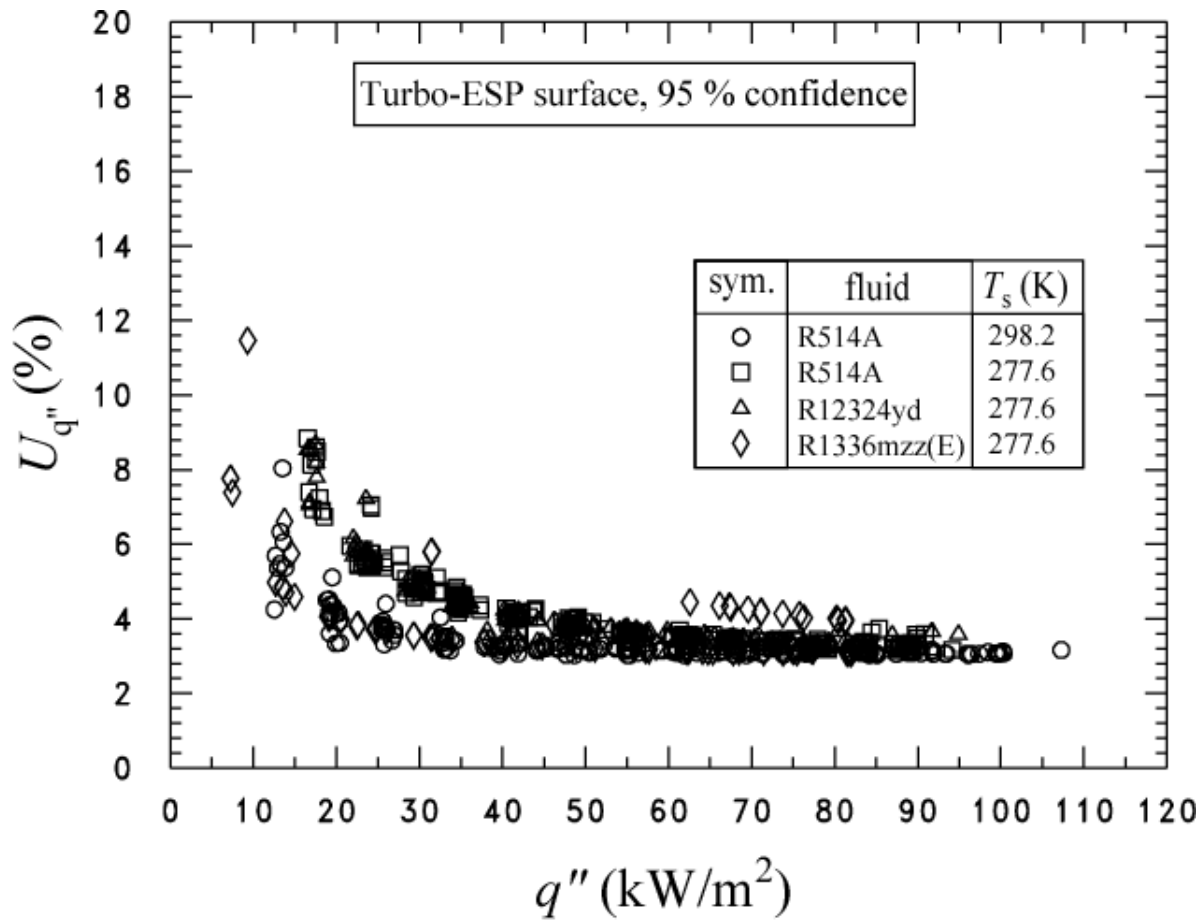


**Fig. A.1 Expanded relative uncertainty in the heat flux of the surface at the 95 % confidence level**

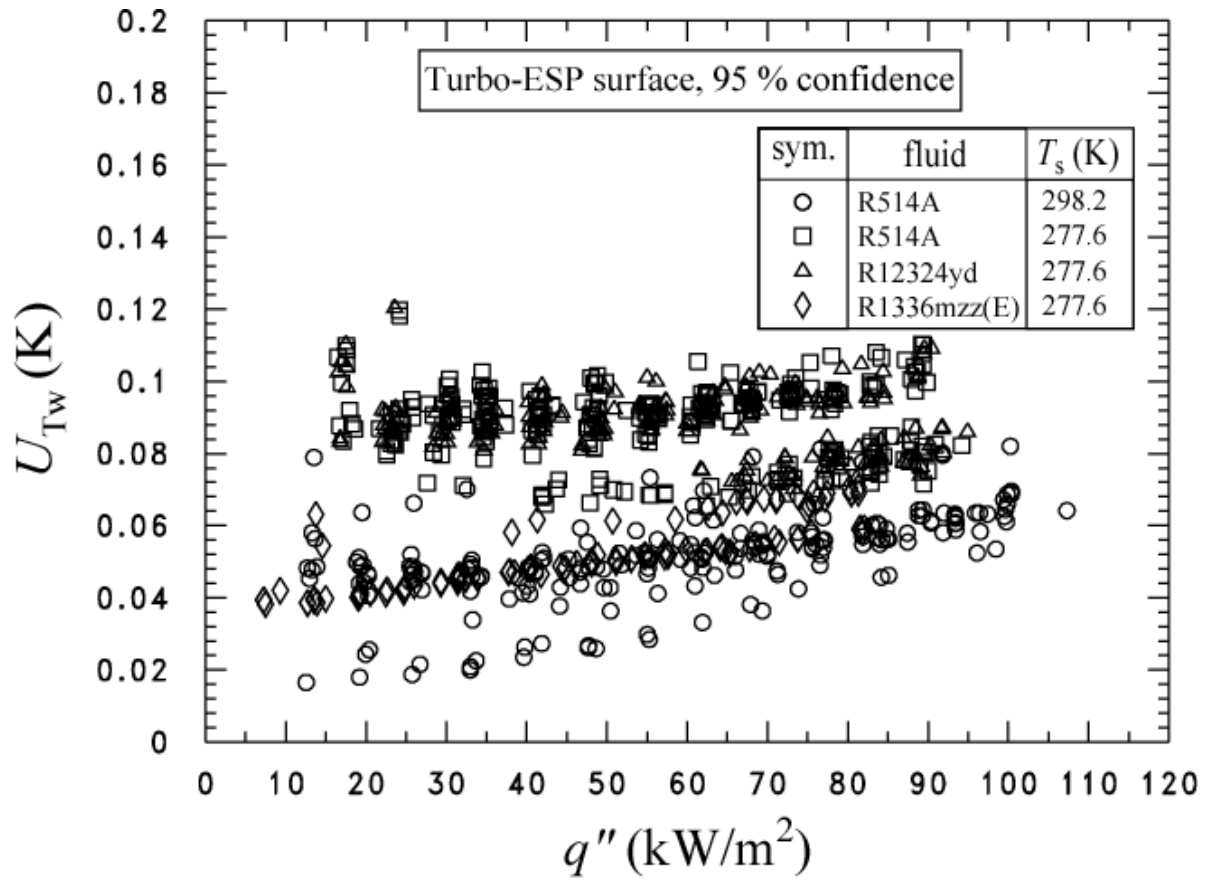


**Fig. A.2 Expanded uncertainty in the temperature of the surface at the 95 % confidence level**